UC San Diego
UC San Diego Previously Published Works

Title

Precision spinal gene delivery-induced functional switch in nociceptive neurons reverses neuropathic pain.

Permalink

Journal

Authors

Tadokoro, Takahiro
Bravo-Hernandez, Mariana
Agashkov, Kirill
et al.

Publication Date

DOI

Peer reviewed

Precision spinal gene delivery-induced functional switch in nociceptive neurons reverses neuropathic pain

Takahiro Tadokoro,[1,2,3,15] Mariana Bravo-Hernandez,[1,15] Kirill Agashkov,[4] Yoshiomi Kobayashi,[1] Oleksandr Platoshyn,[1] Michael Navarro,[1] Silvia Marsala,[1,3] Atsushi Miyanohara,[1,5] Tetsuya Yoshizumi,[1] Michiko Shigyo,[1] Volodymyr Krotov,[4] Stefan Juhas,[6] Jana Juhasova,[6] Duong Nguyen,[6] Helena Kupcova Skalnikova,[6] Jan Motlik,[6] Hana Studenovska,[7] Vladimir Proks,[7] Rajiv Reddy,[8] Shawn P. Driscoll,[9] Thomas D. Glenn,[9] Taratorn Kemthong,[10] Suchinda Malaivijitnond,[10] Zoltan Tomori,[11] Ivo Vanicky,[12] Manabu Kakinohana,[2] Samuel L. Pfaff,[9] Joseph Ciacci,[13] Pavel Belan,[4,14] and Martin Marsala[1,12]

[1]Neuroregeneration Laboratory, Department of Anesthesiology, University of California, San Diego (UCSD), La Jolla, CA 92037, USA; [2]Department of Anesthesiology, University of Ryukyus, Okinawa, Japan; [3]Neurgain Technologies, 9620 Towne Centre Drive, Suite 100, San Diego, CA 92121, USA; [4]Departments of Sensory Signaling and Molecular Biophysics, Bogomoletz Institute of Physiology, Kyiv, Ukraine; [5]Vector Core Laboratory, University of California, San Diego (UCSD), La Jolla, CA 92037, USA; [6]Institute of Animal Physiology and Genetics, Czech Academy of Sciences, Rumburská 89, 277 21 Liběchov, Czech Republic; [7]Institute of Macromolecular Chemistry, Czech Academy of Sciences, Department of Biomaterials and Bioanalogous Systems, Heyrovsky Square 2,162 06 Prague 6, Czech Republic; [8]Department of Anesthesiology, Pain Medicine, University of California, San Diego (UCSD), La Jolla, CA 92037, USA; [9]Gene Expression Laboratory and the Howard Hughes Medical Institute, Salk Institute for Biological Studies, La Jolla, CA 92037, USA; [10]National Primate Research Center of Thailand, Chulalongkorn University, Kaengkhoi District, Saraburi 18110, Thailand; [11]Department of Biophysics, Institute of Experimental Physics, Slovak Academy of Sciences, Kosice, Slovakia; [12]Institute of Neurobiology, Biomedical Research Center, Slovak Academy of Sciences, Kosice, Slovakia; [13]Department of Neurosurgery, University of California, San Diego (UCSD), La Jolla, CA 92037, USA; [14]Kyiv Academic University, Kyiv, Ukraine

Second-order spinal cord excitatory neurons play a key role in spinal processing and transmission of pain signals to the brain. Exogenously induced change in developmentally imprinted excitatory neurotransmitter phenotypes of these neurons to inhibitory has not yet been achieved. Here, we use a subpial dorsal horn-targeted delivery of AAV (adeno-associated virus) vector(s) encoding GABA (gamma-aminobutyric acid) synthesizing-releasing inhibitory machinery in mice with neuropathic pain. Treated animals showed a progressive and complete reversal of neuropathic pain (tactile and brush-evoked pain behavior) that persisted for a minimum of 2.5 months post-treatment. The mechanism of this treatment effect results from the switch of excitatory to preferential inhibitory neurotransmitter phenotype in dorsal horn nociceptive neurons and a resulting increase in inhibitory activity in regional spinal circuitry after peripheral nociceptive stimulation. No detectable side effects (e.g., sedation, motor weakness, loss of normal sensation) were seen between 2 and 13 months post-treatment in naive adult mice, pigs, and non-human primates. The use of this treatment approach may represent a potent and safe treatment modality in patients suffering from spinal cord or peripheral nerve injury-induced neuropathic pain.

INTRODUCTION

Effective treatment of spinal cord or peripheral nerve injury (PNI)-induced neuropathic pain remains a significant clinical challenge.[1,2]

Because the etiology of neuropathic pain is multimodal and can have myriad clinical presentations, there is no universally effective therapy available at present.[3–6] In addition, the most commonly used clinical drugs, even if effective, require a continuous systemic, epidural, or intrathecal delivery to achieve a sustained anti-nociceptive effect and are often associated with supraspinal or spinal-segmental side effects such as sedation or motor weakness.[3] In addition, the use of opioids, which are partially effective for neuropathic pain, can lead to the development of tolerance and potentially to drug misuse or abuse.[7]

While the spinal neuropathic foci originating from local injury or increased afferent input after PNI can somatotopically be identified and compartmentalized to a specific spinal segment(s) and side, the current clinically used treatment strategies/protocols do not permit a spinal segment(s)-restricted delivery of pharmacological agents effective in modulating neuropathic pain. Accordingly, there is an urgent need for the development of a new non-opioid-based anti-nociceptive therapy that would selectively target nociceptive neurons in

affected spinal segments, thus minimizing systemic or regional side effect(s).

In recent years, the use of gene therapy has gained substantial traction as a potential treatment for chronic neuropathic pain. It is expected that the use of adeno-associated virus (AAV) vectors with well-established long-term transgene expression profile encoding anti-nociceptive gene(s) will lead to a long-lasting therapeutic effect.[8] In experimental studies it was demonstrated that intrathecal delivery or a direct parenchymal spinal cord or dorsal root ganglion (DRG) injection of AAV vectors encoding for GAD65 (glutamic acid decarboxylase 65-kDa isoform), miR-7a (microRNA), NaV1.3 (sodium channel 1.3), or NaV1.6 (sodium channel 1.6) knocked out, short hairpin RNA-transient receptor potential cation channel subfamily V member 1 (shRNA-TRPV1) or CBD3 (Ca^{2+} channel-binding domain) is associated with the amelioration of neuropathic pain in rodents.[9–14] There are, however, several limitations in currently used experimental gene therapy-delivery protocols that preclude or limit further pre-clinical and clinical development. First, intrathecal (i.t.) delivery of AAV9 vector leads to an uncontrollable diffusion of a vector in cerebrospinal fluid (CSF) and leads to multi-segmental infection of DRG neurons, as well as retrograde infection of α-motoneurons.[15–17] As such, a segment- and site-targeted transgene expression in spinal nociceptor neurons cannot be achieved by i.t. vector delivery. DRG injection provides segmental specificity; however, the requirement for surgical exposure of multiple DRGs to target 2–3 neighboring spinal segments limits its potential clinical use.[15,18] Second, as previously described, numerous anti-nociceptive gene targets were already tested in experimental studies; however, at present, no gene or genes combination have been identified that would be effective in both selectively suppressing or blocking the activity of developmentally encoded spinal cord excitatory nociceptive neurons and have minimal or no side effects (e.g., sedation, motor weakness).

Under physiological conditions, a fully functional GABA synthesizing-releasing system (mediated primarily by GAD65)[19] and vesicular GABA transporter (VGAT; also called VIAAT [vesicular inhibitory amino acid transporter]) are required for an effective vesicular release of GABA (and glycine) into the synaptic cleft. Whole patch clamp recording on E17.5–18.5 spinal cord motoneurons/spinal cord neurons taken from VGAT knockout mice show a complete loss of GABA and glycine-mediated spontaneous inhibitory post-synaptic currents and a significant decrease in the probability of synaptic vesicular GABA and glycine release.[20,21] These data suggest that a gene therapy aimed at increasing synaptically GABA-mediated neuronal inhibition in the spinal cord (or in the brain) will likely require an exogenously induced expression of both genes (GAD65 and VGAT) to provide a desired therapeutic effect.

To address the limitations in targeted vector delivery, we used a novel subpial vector delivery technique[16,22–24] and have characterized effective vector delivery parameters (vector volume and injection rate), which provide a highly controllable unilateral transgene expression in dorsal horn nociceptive neurons in 2–3 spinal cord segments in adult mice, pigs, and non-human primates (NHPs). Using this delivery technique, we then tested the treatment potency of a subpially delivered combination of two vectors encoding GAD65 and VGAT genes and have demonstrated a complete and long-lasting reversal of sciatic nerve injury-induced neuropathic pain in mice. The therapeutically effective dose of combined vectors was without any detectable systemic or segmental side effects (e.g., sedation, decrease in open field motor performance, change in normal tactile and thermal sensation) in mice, adult pigs, and NHPs for up to 2–13 months post-vector delivery. These data demonstrate a potential use of this new, segment-targeted gene therapy in the treatment of neuropathic pain.

RESULTS

Effective unilateral dorsal-horn-restricted AAV9 vector delivery by targeted subpial AAV injection in mice

In our previous studies, we demonstrated that subpial injections of AAV9 delivered at relatively higher volumes (mouse: 5–10 μL; pig: 200 μL) led to a widespread multi-segmental and bilateral infection of neuronal and glial cells in white and gray matter and retrograde infection-induced transgene expression in neurons in brain motor centers.[16,22–24] Because a targeted expression of therapeutic genes that would be segment and side specific is desired to modulate somatotopically defined neuropathic pain, we tested whether the volume/dose of a subpially delivered AAV vector can be titrated to achieve unilateral and dorsal horn-restricted transgene expression in mice. Adult mice (C57/BL6; n = 12) received unilateral subpial injection of AAV9-UBC (ubiquitin)-GFP (green fluorescent protein; 0.5, 1.0, or 3 μL; n = 3 for each volume) (Figure S1A). After the injection, the animals survived for 14 days.

Unilateral injection of 0.5 μL AAV9-UBC-GFP into lumbar L3–L5 subpial space led to a clear appearance of mRNA-GFP and GFP and was restricted to ipsilateral dorsal horn neurons between L3 and L5 segments (Figures S1A–S1D). No expression in the contralateral side or in the ventral horn was seen. Unilateral injection of higher AAV volumes (1.0 or 3.0 μL) led to a more widespread GFP expression seen in the contralateral side as well as in the ventral horn (Figure S1D).

Analysis of retrograde infection-induced GFP expression in the brain showed only the occasional presence of GFP+ neurons in the brainstem and no GFP+ neurons in the motor cortex in animals receiving 0.5 μL AAV9-UBC-GFP vector. This was in contrast to animals receiving bilateral subpial lumbar (3 + 3 μL) AAV9-UBC-GFP injections, in which intense GFP expression in the brainstem and motor cortex neurons was detected (Figure S1E). Based on these data, the volume of 0.5 μL AAV9 or Anc80 encoding VGAT and/or GAD65 was used in all of the subsequent behavioral efficacy studies in the neuropathic mouse model (Figures 1A and 5A). The AAV-Anc80 vector, which has relatively lower neuronal tropism compared to AAV9, was used, in addition to a well-characterized AAV9, to compare the treatment potency once both transgenes are delivered by using two different delivery vectors.
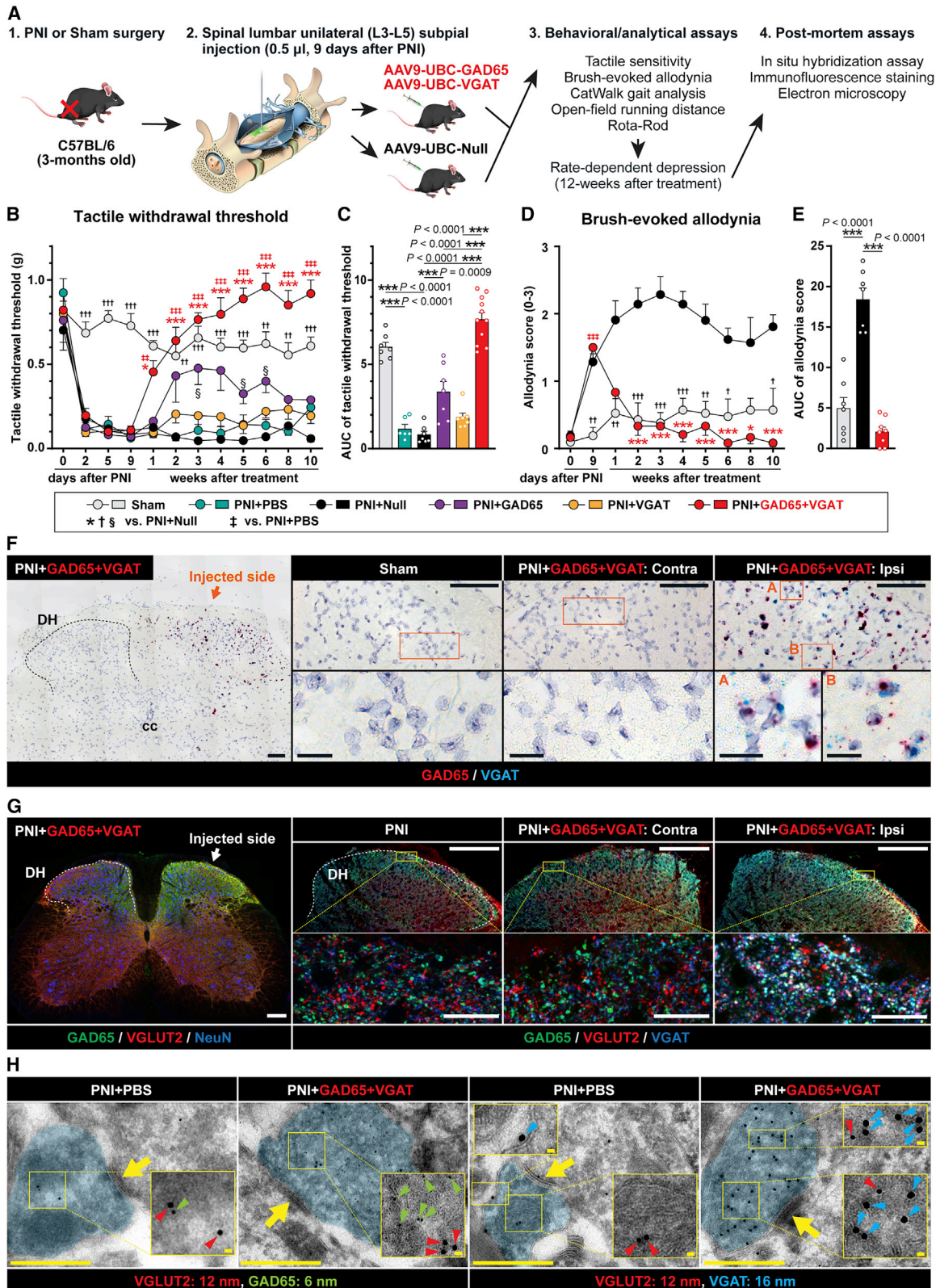
(legend on next page)

Potent reversal of neuropathic pain with preserved normal motor function after unilateral segment-targeted subpial delivery of GAD65 and VGAT genes in mice

Previous studies have demonstrated that GAD65 is the primary enzyme responsible for GABA synthesis in the CNS. It has also been shown that co-expression of VGAT is required for the effective release of VGAT-packaged GABA into the synaptic cleft to achieve a GABA-mediated inhibitory effect on the post-synaptic membrane.[19–21] We, therefore, tested whether the concomitant upregulation of both genes (GAD65 and VGAT) in L3–L5 dorsal horn neurons will lead to a normalization of otherwise increased dorsal horn excitability and suppression of corresponding nociceptive behavior in a mouse model of neuropathic pain (PNI).[25]

To induce neuropathic pain, the sciatic nerve was partially ligated in adult C57BL6 (B6) mice using 6.0 Proline. After sciatic nerve ligation, the presence of pain was identified as tactile stimulus (von Frey filaments) or brush-evoked (dynamic) pain response. At 9 days after sciatic nerve ligation, animals with established neuropathic pain responses received ipsilateral (L3–L5) subpial injection of (1) a mixture of AAV9-UBC-GAD65 + AAV9-UBC-VGAT (referred to as "treatment vectors"), (2) AAV9-UBC-GAD65 only, (3) AAV9-UBC-VGAT only, (4) AAV9-Null (control), and (5) phosphate-buffered saline (PBS) injection only (control). A separate sham-operated group served as an additional control.

The primary efficacy and safety endpoints used in the behavioral component of the study (Figures 1B–1E and 5B–5E) were changes measured in (1) paw tactile withdrawal response, (2) brush-evoked pain response, and (3) open field motor performance. Rotarod performance as well as paw placement pattern (CatWalk) were also tested in a subset of animals to identify any potential fine motor function-related side effect (e.g., paw displacement). All nerve-ligated animals showed a significant decrease in tactile nociceptive threshold as soon as 1 day after sciatic nerve ligation. A comparable increase in brush-evoked pain response was seen. Animals injected with combined treatment vectors showed a progressive loss of pain responses (i.e., increased paw-withdrawal thresholds) starting 7 days after vector delivery and with a complete normalization (i.e., similar to or slightly above pre-injury baseline) of responses in both tactile and brush-evoked tests measured at 14 days (Figures 1B–1E). This treatment effect continued for the duration of the study (10 weeks; Figures 1B–1E). Injection of AAV9-UBC-GAD65 only (without co-injection of AAV9-UBC-VGAT) vector led to a moderate and only transient anti-nociceptive effect (Figures 1B, 1C, and S2A). Injection of AAV9-UBC-VGAT only (without co-injection of AAV9-UBC-GAD65) vector had no significant treatment effect and was similar to PBS-injected and AAV9-Null virus-injected PNI controls (Figures 1B, 1C, and S2A).

Analysis of rotarod and open field motor performance up to 10 weeks post-treatment showed normal motor performance in treated animals that was similar to PNI-AAV9-Null virus and sham-operated animals (Figures S2B, S2C, and S2E). CatWalk analysis of the ipsilateral hind paw digits surface placement showed a clear contracture with the loss in the number of "digit-to-surface" contact points (footprint score) in non-treated neuropathic animals. Neuropathic animals injected with treatment vectors showed a significant normalization of paw digit placement, which was similar to that in control non-injured animals (Figures S2D). Analysis of open field anxiety behavior (which is distinct from the aversive component of pain) showed no detectable difference between sham, PNI-AAV9-Null-injected, and PNI-GAD65 + VGAT-treated animals (Figures S2F).

Assessment of the safety of the combined treatment vector delivery in naive non-injured animals showed a continuing normal tactile and thermal responsivity and open field motor and rotarod performance between 1 and 13 months post-treatment vector injection, which was similar to that of age-matched WT (wild-type) controls (Figures S2G–S2K).

The comparable treatment effect, as measured after treatment with AAV9-UBC-GAD65/VGAT vector, was also seen after using

Figure 1. Spinal unilateral dorsal horn delivery of GAD65 and VGAT genes provides a potent and long-lasting reversal of neuropathic pain

(A) Schematic diagram of the experimental design and "in life" and "postmortem" behavioral/analytical assays. (B–E) Reversal of tactile hypersensitivity (tactile withdrawal threshold), and (D and E) brush-evoked allodynia. Note the progressive appearance of the treatment effect, which correlates with transgene expression and lasts for a minimum of 10 weeks after treatment vector(s) delivery. (F) *In situ* hybridization analysis of L4 dorsal horn using BaseScope probes designed to specifically detect AAV-induced VGAT and GAD65 RNA at 12 weeks after vector(s) delivery. Positive hybridization signals (GAD65: red, VGAT: blue) are detected in the ipsilateral dorsal horn (vector-injected side; Ipsi), but not in the contralateral side (Contra), or in sham-operated animals. (G) Immunofluorescence staining of L3–L5 spinal cord sections with anti-VGLUT2, GAD65, VGAT, and NeuN antibodies at 12 weeks after vector(s) delivery. A clear upregulation of AAV9-encoded transgenes (GAD65 and VGAT) can be identified in the ipsilateral dorsal horn. Analysis of VGLUT2, GAD65, and VGAT in triple-stained sections showed a high density of VGLUT2+ terminals co-expressing GAD65 and VGAT (white signal in the right panel). (H) Immunoelectron microscopy images of L3–L5 spinal dorsal horn neuron-derived terminals after pre-embedding immunogold staining with VGLUT2, GAD65, and VGAT antibodies. In peripheral nerve injury (PNI) non-treated animals, only the occasional presence of GAD65 or VGAT immunogold positive particles is seen in VGLUT2+ terminals. In contrast, animals previously injected subpially with AAV9-UBC-GAD65/VGAT vectors show VGLUT2-containing terminals densely packed with GAD65 and VGAT-stained particles. (B and C) Sham-operated n = 7, PNI + PBS n = 6, PNI + AAV9-Null n = 7, PNI + GAD65 + VGAT n = 11, PNI + GAD65 n = 7, PNI + VGAT n = 7; (B) 2-way repeated ANOVA followed by Tukey's multiple-comparisons test, (C) the area under the curve (AUC) was calculated in arbitrary units from 9 days post-PNI to 10 weeks post-vector injection; Kruskal-Wallis test followed by multiple-comparisons using Dunn's multiple comparisons test. (D and E) Sham-operated n = 7, PNI + AAV9-Null n = 7, PNI + GAD65 + VGAT n = 11; (D) mixed-effects analysis followed by Tukey's multiple-comparisons test, (E) 1-way repeated ANOVA followed by Tukey's multiple-comparisons test. Data are represented as means ± SEMs. Actual p values (left to right): (B) * 0.0125, 0.0002, <0.0001, 0.0002, <0.0001, <0.0001, <0.0001, <0.0001, † 0.0008, <0.0001, 0.0003, <0.0001, 0.0046, 0.0008, 0.0002, 0.0001, 0.0015, 0.0069, 0.0002, ‡ 0.0025, 0.0003, <0.0001, 0.0002, <0.0001, <0.0001, <0.0001, <0.0001, § 0.0315, 0.0225, 0.0197; (D) * 0.0003, 0.0008, <0.0001, 0.0008, <0.0001, 0.0215, <0.0001, † 0.0064, 0.0071, 0.0009, 0.0003, 0.0002, 0.0018, 0.0104, 0.0197, ‡ <0.0001. Scale bars: (F) 100 μm; (F, enlarged images) 20 μm; (G) 200 μm; (G, enlarged images) 20 μm; (H) 500 nm; (H, enlarged images) 20 nm.

another vector variant Anc80-UBC-GAD65 and Anc80-UBC-VGAT (Figures S3B–S3D).

The data demonstrate that ipsilateral dorsal horn delivery of GAD65/VGAT genes by subpial delivery is highly effective in reversing nociceptive responses in the mouse neuropathic pain model. The timing of measurable treatment effect corresponds with the therapeutic gene expression mediated by AAV9 or Anc80 delivery. Reversal of neuropathic pain is associated with the relief of peripheral hind paw digit contractures otherwise seen in non-treated animals. No detectable side effect, such as loss of normal tactile or thermal nociception or decreased motor performance in treatment vector-injected naive animals, was seen for up to 13 months post-injection.

Effective and long-term unilateral dorsal horn upregulation of GAD65 and VGAT mRNAs and proteins in inhibitory and excitatory interneurons after subpial delivery of GAD65 and VGAT genes

We next analyzed the expression pattern of AAV9-mediated GAD65 and VGAT genes in spinal cord neurons. The mice used in the behavioral part of the study were used for immunofluorescence in situ hybridization (FISH; n = 3), immunofluorescence (IF) protein staining (n = 3) and pre-embedding immunohistochemistry (immunogold) coupled with electron microscopy (immuno-EM; n = 2). All of the mice were perfusion fixed between 10 and 12 weeks after vector delivery. In addition, 2 animals were used for IF at 13 months post-treatment and a separate group of animals (n = 12) were used for western blot (WB) analysis at 2 weeks after vector delivery.

In the FISH analysis, two sets of probes were used. First, to identify only the vector-mediated induction of GAD65 and VGAT genes, a double Z probe strategy, which requires a probe pair (ZZ) to simultaneously bind to the target to generate signal, was used in the probe design. Using these probes, we saw specific GAD65 and VGAT signals only in the ipsilateral horn (Figure 1F). In addition, the clear presence of both transgenes in individual dorsal horn cells was identified.

Second, a combination of VGLUT2 (vesicular glutamate transporter), GAD65, and VGAT mouse-specific mRNA probes, which recognizes both endogenous and vector-delivered transgenes, was used. A clear upregulation for both GAD65 and VGAT in ipsilateral (but not in contralateral) dorsal horn neurons was seen (Figure S4A). Numerous VGLUT2 mRNA$^+$ neurons showed co-localization with upregulated GAD65 and VGAT mRNA (Figure S4A). No changes in GAD65 or VGAT mRNA and only occasional colocalization of GAD65 mRNA or VGAT mRNA with VGLUT2 mRNA$^+$ neurons were seen in WT, vector-non-injected animals (Figure S4A).

IF staining with a combination of VGLUT2, GAD65, and VGAT antibodies showed a clear increase in the expression of GAD65 and VGAT protein in the ipsilateral, treatment-vector-injected dorsal horn (Figure 1G). High-power confocal analysis showed the presence of numerous triple-stained VGLUT2/GAD65/VGAT terminals (puncta) (Figure 1G; inserts; light blue to white signal, triple-stained neurons).

Quantitative densitometry analysis using serial sections taken from L2–L6 segments showed a significant ipsilateral increase in both proteins across L3–L5 segments (Figure S4B), while no significant changes were measured in the contralateral dorsal horn.

IF and FISH analysis of spinal cord and DRG sections taken from treatment vector-injected animals at 13 months post-treatment showed an intense transgene (GAD65 and VGAT) expression (IF) in VGLUT2 neurons in ipsilateral dorsal horn, which was nearly identical to that seen at 12 weeks (Figure S4C). Similar continuing upregulation of GAD65 and VGAT mRNA (FISH) in VGLUT2$^+$ DRG neurons was seen in ipsilateral L3–L5 DRGs (Figure S5A). This co-expression was not seen in WT or PBS-injected animals (Figure S5A). WB analysis of spinal cord segments injected previously with both GAD65- and VGAT-encoding vectors (AAV9) showed a significant upregulation of both transgenes at 2 weeks after vector delivery (Figure S5B).

Analysis of DRGs in WT animals injected with AAV9-UBC-GAD65/VGAT and surviving for 10 weeks showed no significant degeneration (as measured by volumetric DRG analysis) or sign of inflammation measured by Iba1 IF (Figures S12A–S12D).

EM analysis in PBS-treated animals revealed the occasional co-presence of VGLUT2 and GAD65 or VGAT$^+$ immunogold particles in the same terminal, and the majority of identified terminals showed the presence of only one protein (i.e., either VGLUT2 or GAD65 or VGAT). In contrast, analysis in AAV9-GAD65/VGAT-treated animals showed numerous VGLUT2 terminals densely packed with GAD65 or VGAT-tagged gold particles (Figures 1H and S6). A quantitative analysis of VGLUT2, GAD65, and VGAT immunogold-stained particles in induced mixed excitatory-inhibitory terminals is presented in Figure S4D.

Animals injected with Anc80-UBC-GAD65 and Anc80-UBC-VGAT showed a comparable presence of triple-stained VGAT/VGLUT2/GAD65$^+$ terminals in the ipsilateral dorsal horn at 8 weeks after subpial vector delivery (Figure S3E).

Suppression of dorsal horn excitatory neuronal circuitry by GAD65 and VGAT upregulation leads to a complete block of rate-dependent depression of the Hoffmann reflex in mice.

Measurement of rate-dependent depression (RDD) of monosynaptic (Hoffmann) reflex is used as an index of spinal inhibitory interneuron recruitment after a progressively increased rate of supramaximal peripheral nerve stimulation (Figure 2A). Under normal conditions, up to 80% reduction in H-reflex amplitude is seen at a 5-Hz stimulation frequency.[26] The RDD was measured in sham-operated, PNI-AAV9-Null-injected, and combined treatment vector-injected PNI animals. The recording was performed at the end of 12 weeks post-vector delivery or of 13 weeks post-sham surgery. In sham-operated and PNI-AAV9-Null-injected animals, a comparable rate-dependent depression of H-wave was seen with ∼80% reduction measured at 5-Hz
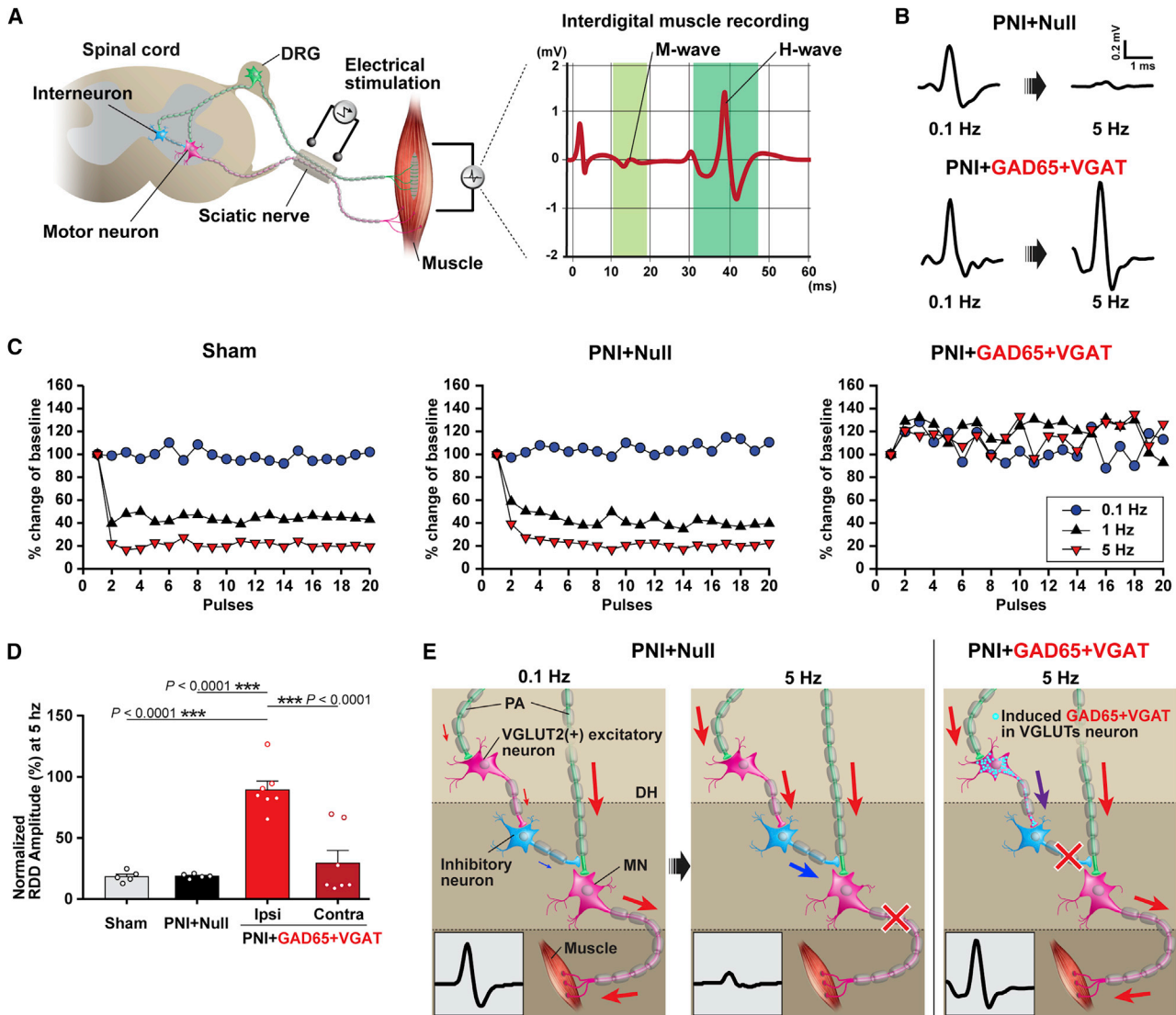
Figure 2. Loss of rate-dependent depression of Hoffmann reflex in neuropathic mice after lumbar subpial AAV9-UBC-GAD65/VGAT delivery

(A) Schematic diagram of H-reflex stimulation and recording. Electrical stimulation of mixed (motor-sensory) peripheral nerve leads to the initial M-wave and is then followed by late spinal monosynaptic reflex-mediated H-wave recorded from interdigital muscle in the hind paw. (B) H-wave amplitudes recorded in neuropathic mice injected with subpial AAV9-Null or AAV9-UBC-GAD65/VGAT vector at 0.1 or 5 Hz stimulation frequency. Note the clear suppression of the H-wave at 5-Hz stimulation frequency in AAV9-Null-injected animals, but not in AAV9-UBC-GAD65/VGAT-treated animals. (C) Comparison of H-wave amplitude(s) between sham-operated, AAV9-Null-injected, and AAV9-UBC-GAD65/VGAT-treated animals at 0.1, 1.0, and 5.0 Hz stimulation frequencies. (D) Quantitative analysis of H-wave amplitude(s) in all experimental groups at 5-Hz stimulation frequency and delivered at H-max intensity. Note a significant loss of rate-dependent depression (RDD) in the ipsilateral (but not in contralateral) side in AAV9-UBC-GAD65/VGAT-injected animals. (E) A diagram depicting a postulated mechanism of RDD suppression in AAV9-UBC-GAD65/VGAT-treated animal. Under physiological conditions (sham-operated or PNI + AAV9-Null-injected), a progressively increased rate of supramaximal nerve stimulation results in the recruitment of dorsal horn (DH) inhibitory interneurons (blue arrow), increased presynaptic inhibition, and resulting decrease in α-motoneuron (MN) activation (red-white cross in center panel) after primary afferent (PA) stimulation. Recruitment of inhibitory interneurons is primarily mediated through VGLUT2^{+} excitatory interneurons. In AAV9-UBC-GAD65/VGAT-treated animals (PNI + GAD65 + VGAT), the excitatory input to inhibitory interneurons is changed to inhibitory, resulting in a block of inhibitory interneuron activation (red-white cross in the right panel) and loss of RDD but with continuing monosynaptic activity (mediated by Ia afferent) evoked α-motoneuron activation. (D) Sham-operated n = 5, PNI + AAV9-Null n = 5, PNI + GAD65 + VGAT n = 7, 1-way repeated ANOVA followed by Tukey's multiple-comparisons test. ***p < 0.001; data are represented as means ± SEMs. DRG, dorsal root ganglion.
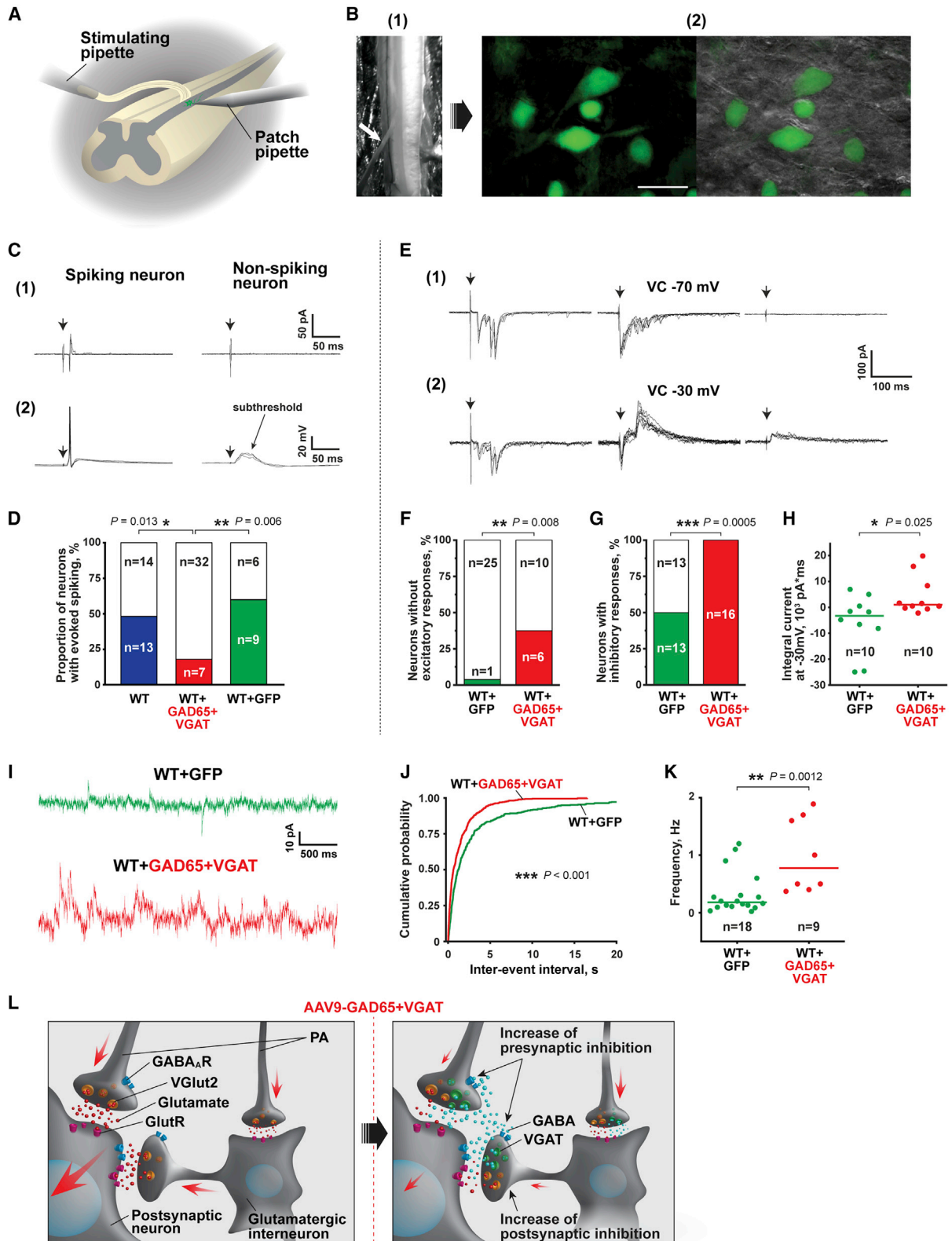
(legend on next page)

stimulation frequency (Figures 2B–2D). In neuropathic pain animals injected with treatment vectors, a complete loss of RDD was observed (Figures 2B–2D). The loss of RDD was seen only in the ipsilateral side, but was still preserved in the contralateral side, suggesting a regional vector-associated effect (Figure 2D). The data suggest a potent block of dorsal horn excitatory circuitry, which is likely mediated by an induced inhibitory neurotransmitter phenotype in primary afferent and/or second-order dorsal horn excitatory interneurons in animals injected with treatment vectors. The data also demonstrate that the monosynaptic reflex mediated by Ia afferents coupled to α-motoneurons is not altered by vector treatment and the effect is restricted to dorsal horn circuitry (Figure 2E).

The upregulation of GAD65 and VGAT in dorsal horn neurons promotes both pre- and post-synaptic inhibition and concomitant reduction in the excitability of the dorsal horn network in spinal cord explants in mice.

Excessive release of GABA due to GAD65/VGAT upregulation may decrease the incidence of action potential (AP) generation in superficial dorsal horn neurons in response to nociceptive stimuli, thus increasing the nociceptive threshold we have measured in the behavioral part of the study. We, therefore, studied the excitability of superficial dorsal horn circuitry, which is involved in nociceptive processing in acutely isolated lumbar spinal cord preparation (Figure 3A). Adult WT mice received a unilateral subpial injection of AAV9-UBC-GFP (1.3×10^{13} genome copies [GC]/mL, 1 μL, n = 6) or a mixture of AAV9-UBC-GAD65 + AAV9-UBC-VGAT + AAV9-UBC-GFP (total 3.0 μL, n = 6). At 2–3 weeks after treatment, vector delivery animals were sacrificed, and the lumbar spinal cord explants with an

attached dorsal root were prepared for patch clamp recordings (Figures 3A and 3B).

We performed cell-attached recordings from dorsal horn neurons of age-matched WT and GFP-infected animals (Figures 3B and 3C [1]). Saturating dorsal root stimuli (1 ms, 150 μA), activating nociceptive Aδ- and C-fiber afferents,[27] produced at least one AP in 48% and 60% of cells from WT and GFP-infected mice, respectively (p = 0.5, Fisher's exact test) (Figure 3D). Thus, the subpial injection and GFP expression did not significantly affect the dorsal horn circuitry. In contrast, the same stimulation mainly evoked subthreshold excitatory post-synaptic potentials (EPSPs) (Figure 3C [2]) and caused spiking in only 18% of cells from GFP/GAD65/VGAT-infected mice, demonstrating that GAD65/VGAT expression significantly suppressed the AP output of the dorsal horn neurons (Figures 3B, 3C [1], and 3D).

We next studied synaptic mechanisms of treatment vector-induced suppression in the excitability of dorsal horn neurons. GAD65 and VGAT expression in VGLUT2+ DRG neurons (Figure S5) is likely to result in a co-release of glutamate and GABA from the central terminals of GAD65/VGAT expressing DRG neurons. This should decrease the evoked EPSPs due to summation with the evoked inhibitory post-synaptic potentials (IPSPs) making the former to be subthreshold. The co-release should also evoke monosynaptic IPSCs and EPSCs with the same latencies after the dorsal root stimulations. In a small part of the experiments (n = 5 of 39, data not shown), we did observe evoked inhibitory currents (recorded at 0 mV), with a narrow jittering in latencies (>2 ms) resembling monosynaptic IPSCs. However, in these dorsal horn neurons, we failed to detect evoked EPSCs having latencies

Figure 3. GAD65/VGAT upregulation promotes inhibition in superficial dorsal horn circuitry, reducing its excitability

(A) Experimental scheme. Intact *ex vivo* spinal cord preparation with an attached dorsal root was used for visually guided patch clamp recordings from Lamina I neurons located in L4–L5 segments of the spinal cord. Spared L5 dorsal root was stimulated via a suction pipette with saturating square pulses of current (1 ms, 150 μA), activating all primary afferents, including nociceptive Aδ- and C-fibers. (B) An image of the intact spinal cord preparation with an attached L5 dorsal root, indicated by a white arrow (1). Images of GFP-expressing neurons in the ipsilateral superficial dorsal horn of mice after subpial delivery of AAV9-UBC-GFP and GAD65/VGAT (2). Left: An epifluorescent image; right: an overlay of epifluorescent and IR LED oblique illumination images. (C) Primary afferent-driven responses of Lamina I spinal cord neurons evoked by saturating dorsal root stimulations (1 ms, 150 μA). Responses of representative spiking and non-spiking neurons recorded in cell-attached (1) and whole-cell current clamp (2) configurations; arrows indicate stimulation artifacts. (D) Proportions of spiking (colored) versus non-spiking (blank) neurons in wild-type (WT), GAD65 + VGAT-infected (WT + GAD65 + VGAT), and sham GFP-infected (WT + GFP) mice. Note the significant suppression in the excitability of dorsal horn neurons in WT + GAD65 + VGAT animals. (E) Evoked post-synaptic currents observed in 3 representative Lamina I neurons in response to the saturating dorsal root stimulations at a holding potential of −70 mV (1) and −30 mV (2) to selectively record EPSCs, EPSCs + IPSCs, and IPSCs, respectively. The neurons responded with EPSCs (left), both EPSCs and IPSCs (center), or IPSCs only (right). Arrows indicate stimulation artifacts. (F) The proportion of neurons lacking (colored) evoked EPSCs was increased in WT + GAD65 + VGAT mice, suggesting the increased presynaptic inhibition within the lamina (I). (G) Proportion of neurons exhibiting (colored) evoked IPSCs was increased in WT + GAD65 + VGAT mice, demonstrating the increased post-synaptic inhibition in the superficial dorsal horn circuitry. (H) Scatter graph depicting integrals of evoked post-synaptic currents (EPSCs + IPSCs) recorded at −30 mV), indicating an inhibition-vectored shift of the excitation/inhibition balance in the dorsal horn of WT + GAD65 + VGAT mice. Dots represent the integral values for individual cells; lines indicate the median values. (I) Examples of spontaneous IPSCs (sIPSCs) recorded in the neurons of WT + GFP (top) and WT + GAD65 + VGAT (bottom) mice at a holding potential of −30 mV. (J and K) GAD65 + VGAT upregulation increased spontaneous inhibitory drive in the superficial dorsal horn. (J) Cumulative probability histogram showing decreased inter-event intervals (s) of GABAergic sIPSCs in WT + GAD65 + VGAT animals. p indicates a result of the Kolmogorov-Smirnov test. (K) Scatter graph showing the increased frequency of sIPSCs in a population of neurons from WT + GAD65 + VGAT mice compared to WT + GFP control. Dots represent the values for individual cells; lines indicate the median values. (L) The proposed scheme of promoted inhibition within the superficial dorsal horn induced by subpial delivery of AAV9-GAD65 and AAV9-VGAT. The activation of secondary nociceptive neurons (post-synaptic neuron) largely relies on the excitatory synaptic drive from VGLUT2+ primary afferents (PA) and VGLUT2+ interneurons (right). GAD65/VGAT expression in these glutamatergic neurons diminishes the excitatory input from primary afferents due to the putative increase in presynaptic inhibition. In its turn, the induction of inhibitory GABAergic phenotype in VGLUT2+ interneurons results in the increase in post-synaptic inhibition. Augmentation of pre- and post-synaptic inhibition in the dorsal horn circuitry suppresses its excitability, decreasing the proportion of neurons, which generate spikes in response to noxious stimuli. *p < 0.05, **p < 0.01, ***p < 0.001; categorical data were analyzed with Fisher's exact test, quantitative data were analyzed with the Mann-Whitney *U* test; n refers to the number of cells analyzed. Scale bars: B (1) 1 mm, B (2) 25 μm.
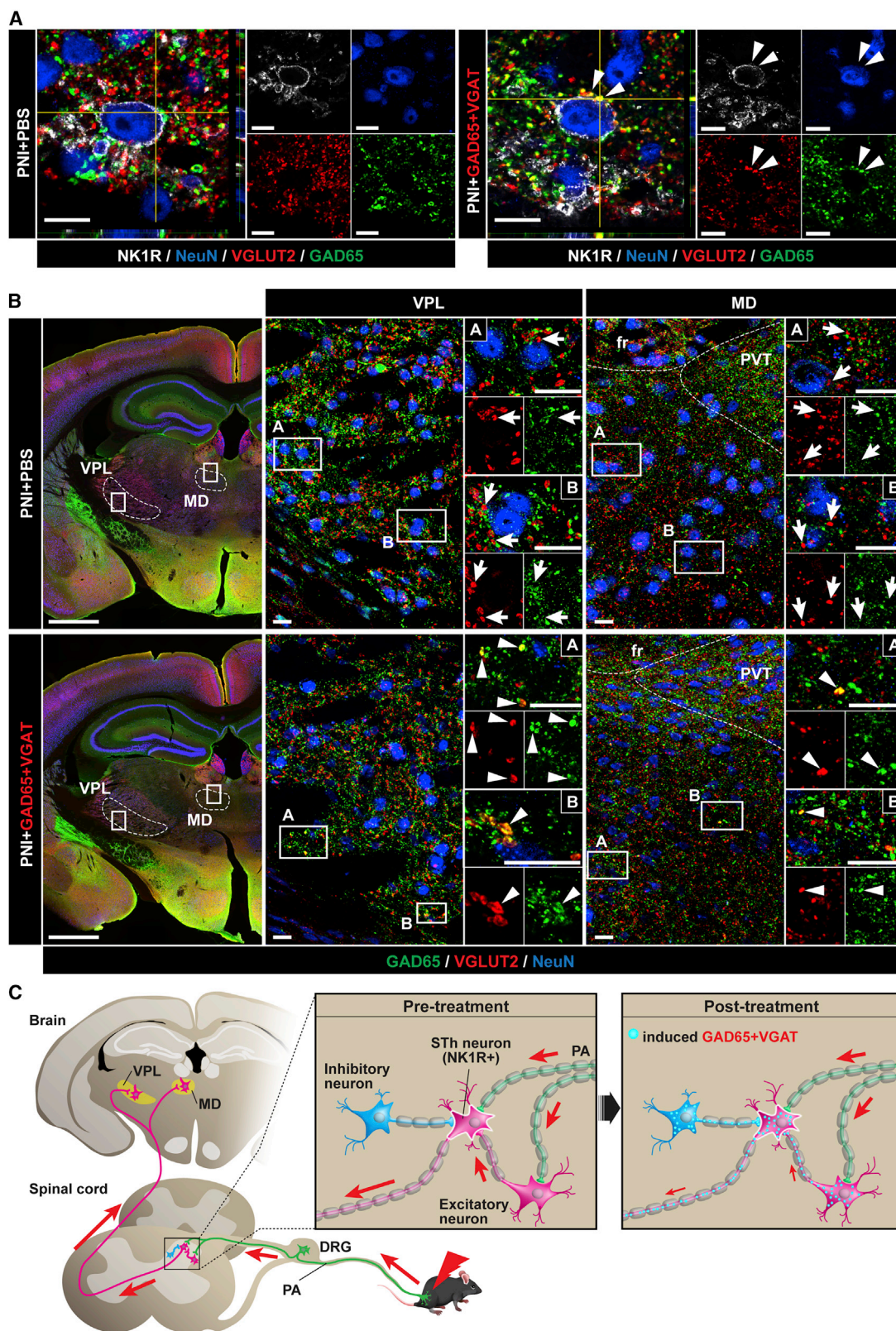
that coincided with IPSCs. Moreover, the application of AMPA (α-amino-3-hydroxy-5-methyl-4-isoxazolepropionic acid)-receptor blocker CNQX (6-cyano-7-nitroquinoxaline-2,3-dione) (10 μM) prevented the evoked IPSCs, with a narrow jittering in latencies (n = 3, data not shown), implying that they were polysynaptic rather than monosynaptic. Altogether, these results indicate that in GAD65/VGAT-infected mice, the central terminals of DRG neurons do not release GABA or released GABA cannot reach $GABA_A$ receptors located on the dorsal horn neurons (Figure 3L). However, we cannot exclude that presynaptic auto-inhibition may contribute to decreased synaptic glutamate release from the primary afferents (Figure 3L).

We next studied whether GAD65/VGAT co-expression in the terminals of glutamatergic dorsal horn neurons (Figures 1H, S6A, and S6B) may evoke a post-synaptic inhibition leading to a decreased excitability of dorsal horn circuitry (Figure 3L). Almost all of the neurons of the WT and GFP-infected mice exhibited complex mono- or/and polysynaptic EPSCs (Figures 3E [1], left, and 3F) in response to saturating dorsal root stimulation reflecting an excitatory synaptic drive from the primary afferents and local neurons, respectively. At the same time, the evoked EPSCs were completely absent in 37% of neurons from GFP/GAD65/VGAT-infected animals (Figures 3E [1], center and right, and 3F), demonstrating that the expression of GAD65/VGAT decreased the excitatory drive to the superficial dorsal horn neurons. The increased proportion of neurons lacking mono- and polysynaptic EPSCs indicates augmented presynaptic inhibition and decreased post-synaptic excitation, respectively.

In WT and GFP-infected animals, saturating dorsal root stimulations induced an inhibitory component of post-synaptic current in 50% of tested neurons, while 100% of cells of GFP/GAD65/VGAT-infected mice exhibited evoked IPSCs (Figures 3E [2], center and right, and 3G), indicating the increased post-synaptic inhibition. Moreover, the outwardly directed inhibitory currents were so robust in these cells that the overall integral of evoked post-synaptic currents became positive (Figure 3H). Thus, exogenous expression of GAD65/VGAT shifted the balance between excitation and inhibition within superficial dorsal horn circuitries toward the inhibition, contributing to the decreased incidence of (AP generation in superficial dorsal horn neurons in response to nociceptive stimuli. This shift was also manifested as an increased spontaneous synaptic inhibitory drive in the local dorsal horn circuitries (Figure 3I). Indeed, a median frequency of spontaneous GABAergic IPSCs recorded in the presence of strychnine

(1 μM) to block inhibitory glycinergic activity was increased in the neurons of GFP/GAD65/VGAT-infected animals (Figures 3J and 3K).

In summary, our electrophysiological data demonstrate that AAV9-induced expression of GAD65 and VGAT in VGUT2$^+$ dorsal horn and potentially in DRG neurons mediates anti-nociceptive effects via promoting both pre- and post-synaptic inhibition and concomitant reduction in excitability of the dorsal horn network, responsible for the processing of nociceptive input (Figure 3L).

Effective induction of mixed excitatory-inhibitory neurotransmitter phenotype in centrally projecting spinal nociceptive pathways after spinal segmental GAD65 and VGAT gene upregulation

A subpopulation of dorsal horn projection neurons plays an important role in nociception, relaying peripheral Aδ and C afferent inputs to the supraspinal centers, thus generating the sensation of pain.[28] Some of these neurons express neurokinin 1 (NK1) receptors[29]. IF analysis of ipsilateral dorsal horn NK1 receptor-positive neurons showed several NK1 receptor-positive neurons receiving mixed VGLUT2/GAD65$^+$ terminals in animals injected with treatment vectors (Figure 4A). This result suggests that the projecting spinothalamic neurons can be subjected to a direct synaptic inhibition induced by the treatment. This may substantially downregulate the output of these nociceptive neurons to the brain, resulting in decreased responsiveness to peripheral nociceptive stimuli. Previous studies have demonstrated that a portion of NK1 neurons represents a population of dorsal horn neurons contributing to anterolateral spinothalamic tract with VGLUT2 terminals projecting to the medio-dorsal (MD) and ventral posterolateral nucleus (VPL) of the thalamus.[30] In addition, the Lamina I nociceptive neuron (targeted by treatment vectors) contributes to the formation of the pain-specific spino-parabrachial (lateral parabrachial nucleus; LPb) and spinal-periaqueductal gray (PAG) pathways. Analysis of all Lamina I neuron-projecting regions, including MD, VPL, LPb, and PAG, showed numerous VGLUT2/GAD65 co-expressing terminals in animals injected with treatment vectors. No colocalization of VGLUT2 with GAD65 or VGAT was seen in PBS-injected animals (Figures 4B and S11A–S11C).

These data demonstrate an effective induction of the mixed excitatory-inhibitory neurotransmitter phenotype in segmental but also in spinothalamic, spino-parabrachial, and spino-PAG area-projecting dorsal horn neurons after local subpial AAV9-GAD65/VGAT delivery.

Figure 4. The induced inhibitory phenotype in pre- and post-synaptic spinothalamic pathway after lumbar subpial AAV9-UBC-GAD65/VGAT delivery
(A) Compared to PBS-injected animals (left panel; PNI + PBS), an NK1 receptor-positive neuron receiving VGLUT2 contacts which co-express GAD65 can be seen in the dorsal horn (right panel; PNI + GAD65 + VGAT; white arrowheads). (B) Analysis of thalamic regions (ventral posterolateral nucleus [VPL] and mediodorsal thalamus [MD]) receiving terminals of spinothalamic (STh) neurons showed the presence of mixed VGLUT2$^+$ projecting terminals co-expressing GAD65 in animals injected subpially with AAV9-UBC-GAD65/VGAT (bottom panel; PNI + GAD65 + VGAT; white arrowheads). (C) A diagram depicting a postulated contribution of the spinothalamic pathway in anti-nociceptive action measured after dorsal horn GAD65/VGAT gene upregulation. Under physiological conditions, the nociceptive stimulus is transmitted to NK1 receptor-positive dorsal horn neurons (i.e., spinothalamic tract forming neuron) from primary afferents (PA) or excitatory VGLUT2$^+$/NK1 receptor$^-$ interneuron. The signal is then transmitted to thalamic nuclei through the spinothalamic pathway. Spinal subpial delivery of AAV9-UBC-GAD65/VGAT leads to the induction of the GABAergic inhibitory phenotype in primary afferents, VGLUT2$^+$/NK1 receptor$^-$ interneurons, and in NK1 receptor$^+$ projecting STh neurons, all of which may contribute to the observed anti-nociceptive effect. PVT, paraventricular thalamus, fr, *fasciculus retroflexus*. Scale bars: (A) 10 μm; (B) 1 mm; B (enlarged images) 20 μm.

A

1. Peripheral nerve injury (PNI)

WT (C57BL/6)   Vgat-cre   Vglut2-cre

Tactile sensitivity
Brush-evoked allodynia

2. Spinal lumbar subpial injection
(0.5 µl, 9 days after PNI)
AAV9-Lox-PLox2272-GAD65
AAV9-Lox-PLox2272-VGAT

Tactile sensitivity
Brush-evoked allodynia

3. Post-mortem assays
(10-weeks after treatment)
Immunofluorescence staining
FISH

B Tactile withdrawal threshold

C
$P = 0.0002$
$P < 0.0001$

D Brush-evoked allodynia

E
$P = 0.0002$
$P < 0.0001$

○ WT+PNI+ floxed-GAD65+VGAT
● Vgat-cre+PNI+ floxed-GAD65+VGAT
● Vglut2-cre+PNI+ floxed-GAD65+VGAT
* vs. Vgat-cre+PNI+ floxed-GAD65+VGAT
† ‡ vs. WT+PNI+ floxed-GAD65+VGAT

F

Vgat-cre + PNI + PBS   Vgat-cre + PNI + floxed-GAD65+VGAT   Vglut2-cre + PNI + PBS   Vglut2-cre + PNI + floxed-GAD65+VGAT

VGAT / VGLUT2 / GAD65

G

VGlut2   GAD65   VGAT

Vgat-cre+PNI+ floxed-GAD65+VGAT
Vglut2-cre+PNI+ floxed-GAD65+VGAT

H

Vglut2-cre + PNI + PBS   Vglut2-cre + PNI + floxed-GAD65+VGAT   Vglut2-cre + PNI + PBS   Vglut2-cre + PNI + floxed-GAD65+VGAT

GAD65 / VGLUT2 / DAPI   VGAT / VGLUT2 / DAPI

(legend on next page)

Jointly, these data support a possibility that the anti-nociceptive effect seen in GAD65/VGAT-treated PNI animals resulting in part from the induced inhibitory neurotransmitter phenotype is centrally projecting VGLUT2(+) spinal nociceptive neurons.

The anti-nociceptive effect measured after targeted dorsal horn GAD65 and VGAT genes delivery is primarily mediated by the induction of the preferential inhibitory phenotype in dorsal horn excitatory nociceptive interneurons.

As demonstrated, the unilateral spinal dorsal horn delivery of GAD65 and VGAT genes has a highly potent anti-nociceptive effect and corresponds with the overexpression of both transgenes in inhibitory and excitatory dorsal horn interneurons. This pattern of transgene expression suggests that the observed potentiation in the dorsal horn neuronal inhibitory activity can be the result of (1) the increased inhibitory potency of local GAD65/VGAT-overexpressing inhibitory interneurons or (2) the induction of the mixed inhibitory-excitatory phenotype in endogenous excitatory VGLUT2$^+$ neurons (as demonstrated by patch clamp analysis and IF and EM assays). To study a relative contribution of treatment-vector-infected inhibitory versus excitatory neurons in observed anti-nociceptive effects, we next used VGLUT2-Cre or VGAT-Cre mice and tested the anti-nociceptive effect after unilateral subpial delivery of GAD65-Lox and VGAT-Lox AAV9 vectors in animals with sciatic nerve ligation-induced neuropathic pain (Figure 5A).

Delivery of "loxed" treatment vectors in VGAT-Cre mice had no detectable anti-nociceptive effect for the duration of the study (8 weeks). In contrast, a potent suppression of tactile stimulus-evoked nociceptive response and brush-evoked allodynia was observed in VGLUT2-Cre mice (Figures 5B–5E). The potency and the time course of this treatment effect were nearly identical to that seen in WT neuropathic animals receiving AAV9-UBC-GAD65/VGAT vectors (shown in Figures 1B–1E).

Confocal microscopy and quantitative analysis confirmed a high specificity of Cre-Lox recombination when the upregulation of GAD65 and VGAT was only seen in VGAT-expressing dorsal horn neurons (terminals) (Figure 5F; second panel from left; light blue signal) in VGAT-Cre animals. In the same VGAT-Cre animals, no recombination in VGLUT2 neurons was detected when no GAD65 and VGAT transgene expression in VGLUT2 terminals (as evidenced by the unchanged VGLUT2 staining pattern similar to that of control PBS-injected animals) was seen (Figure 5F; second panel from left; red signal). In contrast, analysis of GAD65 and VGAT expression in VGLUT2-Cre mice showed selective expression of one or both of the transgenes in VGLUT2 terminals only (Figure 5F; first panel from right; white signal, both transgenes expressed in VGLUT2 terminals; pink or yellow signal, GAD65 or VGAT transgene expressed in VGLUT2 terminals, respectively). In the same animals, no change in VGAT staining pattern in endogenous neuron-derived VGAT terminals was seen (compared to PBS-injected animals) (Figure 5F; first and second panel from right; green signal), confirming selective recombination in VGLUT2 terminals only. Analysis of DRG neurons in VGLUT2-Cre animals similarly showed upregulation of both transgenes in VGLUT2$^+$ DRG neurons (Figure 5H).

These data demonstrate that the observed therapeutic anti-nociceptive effect is primarily mediated by the induction of preferential inhibitory phenotypes in endogenous dorsal horn excitatory VGLUT2$^+$ nociceptive interneurons.

The anti-nociceptive effect measured in animals treated with GAD65/VGAT vectors is independent of ongoing spinal cord microglial (and astrocyte) activation

Previous studies have demonstrated that the activation of spinal microglia after PNI plays a role in the initiation and maintenance of neuropathic pain.[31–34] To analyze the activation status of dorsal horn microglia and astrocytes, mRNA sequencing was performed on dorsal horn extracts taken from: (1) WT non-treated animals, (2) empty vector-injected PNI animals, and (3) GAD65/VGAT-injected PNI animals. In comparison to WT animals, an upregulation of several microglia-activation-associated (C4b, CCl12, Fcgr2b, Fcgr1) and astrocyte-associated (GFAP, Slc14a1, Aqp4) genes was measured in neuropathic pain animals injected with empty vector. Similar upregulation of both microglial and astrocyte-associated genes in GAD65/VGAT-treated animals was seen. These data

Figure 5. The anti-nociceptive effect after subpial AAV9-UBC-GAD65/VGAT delivery is mediated by induction of inhibitory neurotransmitter phenotype in excitatory VGLUT2$^+$ nociceptive neurons

(A) Schematic diagram of the experimental design using neuropathic WT, Vgat-ires-Cre (VGAT-Cre), and Vglut2-ires-Cre (VGLUT2-Cre) mice injected subpially with AAV9-Lox-PLox2272-GAD65/VGAT vectors and in life and postmortem behavioral/analytical assays. (B–E) Analysis of tactile withdrawal threshold and brush-evoked allodynia showed a potent anti-nociceptive effect in treatment vector-injected VGLUT2-Cre mice, but it was without effect in VGAT-Cre and WT mice. (F and G) Qualitative and quantitative immunofluorescence analysis of L3–L5 spinal cord sections stained with anti-VGLUT2, GAD65, and VGAT antibodies showed a significant increase in both transgenes (GAD65 and VGAT) in the ipsilateral dorsal horn. In VGAT-Cre mice, no GAD65 or VGAT immunoreactivity in VGLUT2$^+$ terminals can be seen. In contrast, a high density of triple-stained VGLUT2/GAD65/VGAT terminals in VGLUT2-cre mice can be identified (F; right panel, white signal). (H) Fluorescence in situ hybridization (FISH) analysis of L3–L5 DRG neurons in VGLUT2-Cre mice showed an intense mRNA-GAD65 and VGAT in mRNA-VGLUT2$^+$ neurons. Only some neurons showed co-mRNA-GAD65/VGAT/VGLUT2 presence in PBS-injected animals. (B–E) WT + PNI + floxed-GAD65 + VGAT n = 7, VGAT-Cre + PNI + floxed-GAD65 + VGAT n = 8, VGLUT2-Cre + PNI + floxed-GAD65 + VGAT n = 8. (B and D) Two-way repeated ANOVA followed by Tukey's multiple-comparisons test. (C and E) The AUC was calculated in arbitrary units from 9 days post-PNI to 8 or 6 weeks post-vector injection, 1-way ANOVA followed by Tukey's multiple-comparisons test. (G) n = 3 mice per each group, 3 random sections from L3 segment for each animal. Kruskal-Wallis test followed by multiple comparisons using the Mann-Whitney U test with Bonferroni adjustment. $^*p < 0.05$, $^{**}p < 0.01$, $^{***}p < 0.001$. Data are represented as means ± SEMs. Actual p values (left to right): (B) * 0.0149, 0.0056, 0.0027, 0.0026, 0.0003, 0.0026, 0.0466, † 0.0074, 0.0441, 0.0049, 0.0137, 0.0069, 0.0234, ‡ 0.0247; (D) * 0.0007, 0.0008, 0.0009, † 0.0167, 0.0003, <0.0001. Scale bars: (F and H) 100 μm; (F and H enlarged images) 20 μm.
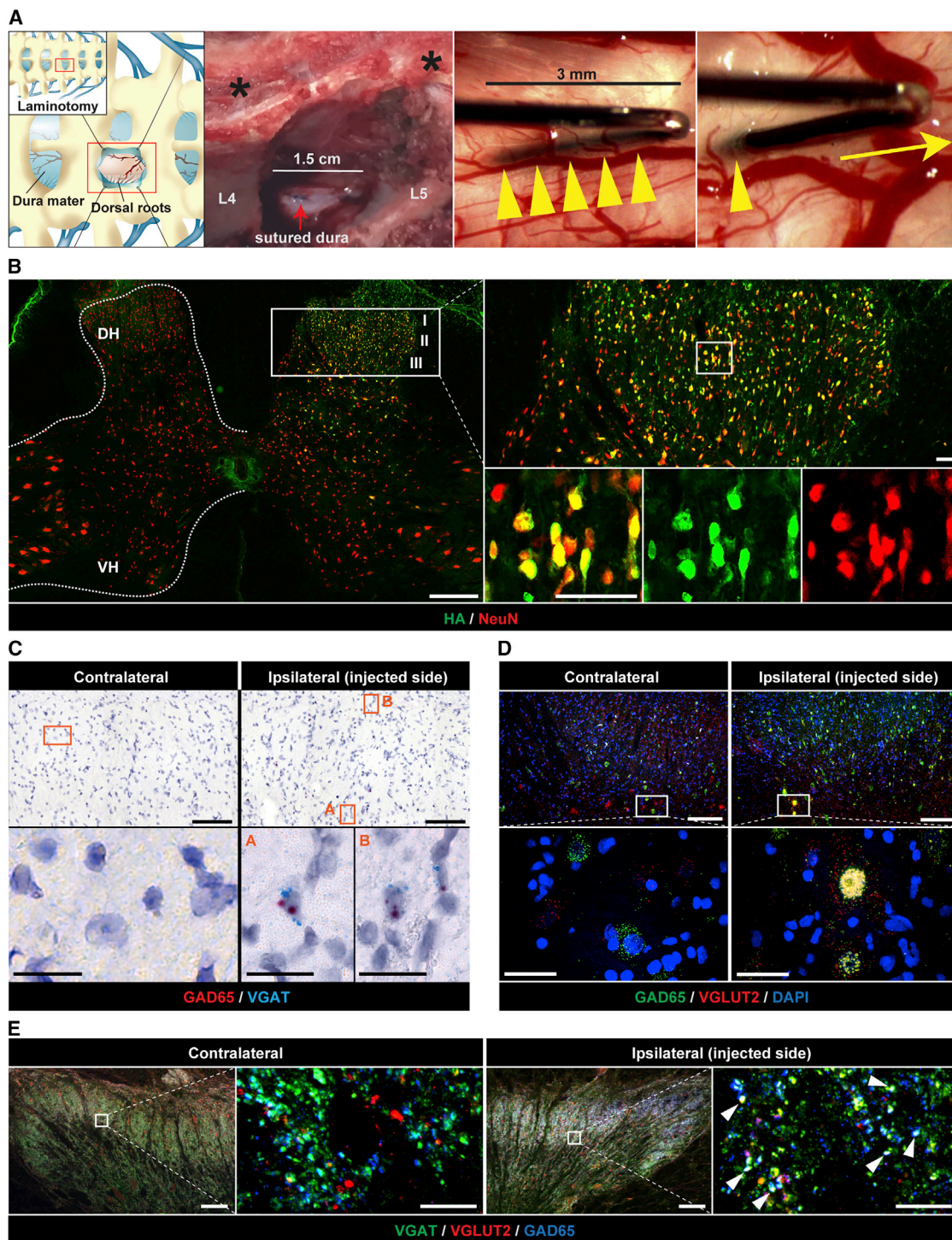
Figure 6. Effective unilateral dorsal horn Anc80 vector delivery in adult naive minipigs

(A) Schematic diagram and intraoperative photographs depicting a partial unilateral laminotomy of L3 and L4 vertebrae and the placement of 27-G "pencil-style" needle into the subpial space just before and after a single bolus vector delivery. Note that spinal processes are not removed (black asterisks). (B) Analysis of Rpl22 protein (3xHA-tagged) expression at 48 h after unilateral subpial delivery of Anc80-UBC-Rpl22-3xHA vector (100 μL). Note an ipsilateral expression (green signal) of Rpl22 protein, which is restricted to dorsal horn (Laminae I–III) neurons. (C) BaseScope *in situ* hybridization analysis of L4 dorsal horn using vector-transgene-specific probes designed to detect only

(legend continued on next page)

demonstrate that the anti-nociceptive effect measured in animals treated with GAD65/VGAT vectors is independent in ongoing spinal cord microglial (and astrocyte) activation (Figures S7A and S7B).

Effective unilateral subpial GAD65 and VGAT genes delivery in adult naive pigs and NHPs using a human subpial injection device

We next developed preclinical large animal data to define the optimal volume of viral subpial injectate that would target only dorsal horn neurons in selected spinal segments and to establish the safety profile of the intended human Anc80-GAD65/VGAT viral dose. A minimally invasive neurosurgical approach, which requires only small unilateral laminotomy (∼1.5 cm in length) to gain access to subpial space at targeted spinal segments, was developed when spinous processes are not removed. Using this approach, the dura is cut open (∼1-cm-long opening) to permit the placement of a subpial needle (3-mm-long subpial needle arm) using an XYZ manipulator and a surgical microscope (Figure 6A).

We performed comparative analysis using available spinal cord anatomical dimension(s) data in adult mice (B6), NHPs (Rhesus macaque), humans, and pigs (Gottingen-Minnesota; 20–25 kg and 80 kg) (Figures S8A and S8B), and have estimated the volume of viral vector to be used in different animal species and humans. Based on these comparative data, we have determined that the volume of subpial vector injection in the 20 to 25 kg pig is between 50 and 200 μL and in adult rhesus monkeys with 3–5 kg total body weight (BW) it is ∼25–50 μL (Figure S8B). Accordingly, to study the rostro-caudal and dorsoventral distribution of subpially delivered vector adult pigs (n = 9; 20–25 kg), they received 50, 100, or 200 μL virus (Anc80 encoding Rpl22-3xHA) unilaterally into the subpial space of the L4–L5 segments and survived for 2 days. Qualitative and quantitative analyses of hemagglutinin (HA)-expressing cells showed that the unilateral delivery of 100 μL of the vector is effective in infecting unilateral dorsal horn NeuN (hexaribonucleotide binding protein-3)-positive neurons localized between Laminae I–III/IV in the L4–L5 segments (Figures 6B, S9A, and S9B).

Based on these initial screening data, we next tested the safety of unilateral subpial (L3–L5) delivery of Anc80-UBC-GAD65/VGAT (100 μL) in adult pigs (25–30 kg; n = 4). After virus injections, the animals survived for 8 weeks. The open field motor assessment showed no detectable deficit in any animal. Measurement of the skin twitch response after applying mechanical stimulus into the outer ipsilateral thigh showed a normal response in all of the animals at 8 weeks post-vector injection.

Using vector transgene-specific probes (targeting GAD65 and VGAT), we found that the FISH analysis showed a clear presence of both transgenes (GAD65 and VGAT) in ipsilateral dorsal horn

cells (Figure 6C). Additional FISH analysis, using a combination of VGLUT2, GAD65, and VGAT mRNA probes, which recognizes both endogenous porcine and vector-delivered transgenes, showed a clear presence of GAD65 in VGLUT2$^+$ neurons in the same ipsilateral dorsal horn regions (Figure 6D).

IF analysis of VGAT/GAD65/VGLUT2-stained lumbar spinal cord sections showed the presence of VGLUT2/VGAT and VGLUT2/GAD65 co-expressing terminals, which were ipsilateral to the side of treatment vector injections (Figure 6E).

Similarly, the safety of unilateral (L4–L5) subpial delivery of Anc80-UBC-GAD65/VGAT (25 μL) in adult cynomolgus monkeys (3–5 kg; n = 5) was studied, with animal survival for 8 weeks. No detectable changes in open field motor function or hindlimb pinch response was seen in any animal at 8 weeks post-subpial injection. FISH analysis using vector-specific transgene(s) probes recognizing GAD65 and VGAT showed (as was seen in mice and pigs) the presence of both transgenes containing cells in the ipsilateral dorsal horn. Comparably, FISH analysis using a combination of VGLUT2, GAD65, and VGAT mRNA probes, which recognize both endogenous NHP and vector-delivered transgenes, showed a clear presence of VGAT transcript in VGLUT2$^+$ neurons in the ipsilateral dorsal horn (Figures S10A and S10B).

IF analysis of spinal cord sections showed the presence of VGLUT2$^+$ terminals co-labeled with GAD65 and VGAT in the ipsilateral (but not contralateral) dorsal horn neurons in treatment vector-injected segments (Figure S10C).

These data demonstrate that the subpial delivery of Anc80-GAD65/VGAT at an intended human dose, surgical approach, and injection device to be used in an adult human is safe and has no detectable functionally defined side effect for a minimum of 2 months after treatment vector delivery.

DISCUSSION

We demonstrated that a subpial unilateral dorsal horn-targeted delivery of a combination of GAD65 and VGAT-encoding AAV vector(s) is highly potent in reversing neuropathic pain long term in a mouse model of sciatic nerve injury. The expression of both transgenes (GAD65 and VGAT) is restricted to the ipsilateral dorsal horn of injected lumbar segments and has no detectable side effect (e.g., motor weakness, loss of normal sensation) in adult naive mice, pigs, and NHPs for up to 2–13 months after vector delivery. The expression of both genes was required to induce a therapeutic effect, while the overexpression of the GAD65 or VGAT gene had no or only a moderate and transient anti-nociceptive effect. The similar partial anti-nociceptive effect after direct DRG injection of rAAV-GAD65 in a

---

AAV-induced VGAT and GAD65 RNA (but not endogenous) at 8 weeks after unilateral Anc80-UBC-GAD65/VGAT delivery (100 μL). Both positive hybridization signals (GAD65: red, VGAT: blue) are detected in ipsilateral dorsal horn in the same cells, but not in contralateral side. (D) FISH analysis of L4 dorsal horn shows colocalization of GAD65 and VGLUT2 mRNA in Lamina IV neurons in ipsilateral dorsal horn. (E) Co-expression of GAD65 and VGAT proteins in VGLUT2$^+$ terminals in ipsilateral dorsal horn. Scale bars: (B) 500 μm; (B enlarged images) 50 μm; (C and D) 100 μm; (C and D enlarged images) 20 μm; (E) 200 μm; (E enlarged images) 50 μm.

rat model of neuropathic pain has been previously reported.[9] Jointly, these data are consistent with previously established observations that the co-expression of both GAD65 and VGAT genes in presynaptic neurons is required to generate a synaptically mediated inhibitory effect.[19–21]

Interestingly, in the present study, the nociceptive threshold was slightly increased over the pre-injury baseline in PNI animals after treatment, but not in naive controls. We speculate that it can be due to increased AAV transduction potency in chronic nociceptive-afferent-input-activated neurons. It is also possible that lower vector titers will be sufficient to achieve the desired clinically defined treatment effect.

By using VGLUT2-Cre and VGAT-Cre mice, we have demonstrated that the primary mechanism leading to the anti-nociceptive effect in animals injected with both treatment vectors results solely from the induced inhibitory phenotype in excitatory (VGLUT2^{+}) dorsal horn neurons. Previous studies have demonstrated the existence of neurons in the ventral tegmental area and entopeduncular and supramammillary nuclei, which co-release glutamate and GABA by distinct VGLUT2 and VGAT vesicles from the same axonal terminal. It was also shown that these "mixed" excitatory-inhibitory axonal terminals simultaneously establish asymmetric (AMPA glutamate receptor-excitatory) and symmetric (GABA$_A$ receptor-inhibitory) synapses with post-synaptic neurons.[35,36] Our quantitative EM analysis showed a similar presence of VGLUT2/VGAT co-expressing terminals in dorsal horn neurons in naive non-treated animals. In therapeutic vector(s)-injected animals, a more than 10-fold increase in the ratio of GAD65/VGAT versus VGLUT2 immunoreactive vesicles in terminals was seen, confirming a highly potent induction of prevalent inhibitory phenotypes in dorsal horn VGLUT2 excitatory interneurons. In addition to the behaviorally defined treatment effect, these immunostaining data correlated with a profound increase in inhibitory activity as measured by single-cell patch clamp recordings from treatment vector-infected second-order dorsal horn neurons after primary afferent stimulation.

Jointly, these data demonstrate that by the exogenous delivery of GABA inhibitory machinery into excitatory nociceptive neurons, it is possible to achieve a functional switch in developmentally "hardwired" excitatory nociceptive systems and that there is no detectable compensatory endogenous mechanism that would lead to a reversal of this treatment vector(s)-induced effect. The population of excitatory dorsal horn neurons targeted by this therapy represents regional interneurons and spino-thalamic-, spino-parabrachial-, and spinal-PAG-projecting neurons.

The mechanism of this treatment effect (i.e., neuron-phenotypic switch) can have a potential significant implication once used in the treatment of neuropathic pain of a different etiology. It has been well established that nociceptive afferent input (as seen in PNI or inflammation- or spinal injury-induced pain) leads to the activation of spinal microglia, astrocytes, and regional monocytes that directly contribute to the initiation and/or maintenance of the neuropathic pain state.[31–34] The mechanism of this effect is associated with an increase in the extracellular release of several neuromodulators (e.g., proinflammatory cytokines including: interleukin-1 β, interleukin-6, and tumor necrosis factor-α,[37–41] or prostaglandins)[42–44] and the resulting potentiation of the excitability of spinal nociceptive neurons after peripheral stimulation.

In the present study, using mRNA sequencing analyses of the dorsal horn, we have demonstrated a continuing upregulation of neuropathic pain-associated microglial/astrocyte genes in both treated pain-free animals and non-treated neuropathic pain animals at 3 months post-vector delivery. This is consistent with the unchanged pre-synaptic primary afferent excitatory input we have measured in dorsal horn patch clamp recordings after primary afferent stimulation in treated animals. Jointly, these data demonstrate that the treatment effect we have observed in our study (1) is primarily based on changed excitatory to the inhibitory phenotype of spinal second-order nociceptive neurons (but not in primary afferents), and (2) is independent of ongoing dorsal horn microglial activation. As such, the technology of the "neuron phenotypic switch" in spinal nociceptive neurons may represent a universal treatment strategy for neuropathic pain induced and/or maintained by different pathophysiological mechanism(s).

One of the prerequisites for clinically acceptable anti-nociceptive therapy is a minimal or complete lack of side effect(s), such as general sedation, motor weakness, or development of tolerance. In addition, a single treatment intervention that provides a long-lasting treatment effect would represent a highly desirable treatment approach (technology).

Our long-term safety study showed that there is no detectable decrease in motor performance (indicative of motor weakness) or loss or normal tactile or thermal sensation for up to 13 months in naive-treatment vector-injected mice. Similarly, no detectable side effect was seen in adult pigs and NHPs injected at the intended human vector dose (GAD65 and VGAT) and that lead to a comparable induction of mixed excitatory-inhibitory neurotransmitter phenotypes in L4–L6 dorsal horn neurons at 2–3 months post-injection. We also demonstrate that the unilateral delivery of vectors into the lumbar spinal cord of adult pigs using newly designed human spinal subpial injection devices can be achieved with small (1.5-cm-long) unilateral partial laminotomy (i.e. without removal of spinal processes). Accordingly, this injection procedure can be performed routinely by any well-trained spinal neurosurgeon.

In summary, we demonstrate that the spinal-unilateral subpial delivery of GAD65 and VGAT genes is highly effective in providing a potent and long-lasting reversal of PNI-induced neuropathic pain. The mechanism of this anti-nociceptive effect is the result of the induced neurotransmitter-phenotypic switch from excitatory to inhibitory in dorsal horn nociceptive neurons.

No detectable side effect(s) such as sedation or motor weakness for up to 2–13 months post-vector injection in adult mice, pigs, and NHPs suggests that this "precision neurology approach," which permits

the unilateral delivery of treatment vectors into selected spinal segments can represent a novel approach for the treatment of neuropathic pain. In addition, because the treatment effect was found to be independent of the activity or regional neuromodulators (associated with local microglial activation), this treatment approach can have broad applicability in the treatment of a wide spectrum of neurological disorders associated with neuronal hyperactivity. This may include spinal injury-induced muscle spasticity, inflammation-induced spinal hyperreflexia, and/or epilepsy.

MATERIALS AND METHODS

Preparation of viral vectors

Self-complementary AAV (scAAV9 or scAAV-Anc80) constructs expressing GFP, GAD65, and VGAT driven by the UBC promoter were made by DNA synthesis of the UBC promoter (1.2 kb) through GFP (720 bp), GAD65 (1.8 kb; rat sequence), or VGAT (1.6 kb; rat sequence) and cloning them into a scAAV backbone plasmid, respectively. Rat GAD65 cDNA (NM_012563.2): NCBI reference sequence: GenBank: M72422.1. GI (sequence identification number): 204225, 5′ tagcagaacccATGGCATCTCCGGG— —CAAGATTTGTAAtcactttgc tcaccaaactttcagtt 3′ (upper case: coding sequence, lower case: flanking sequence). Rat VGAT cDNA: NCBI reference sequence: GenBank: AF030253.1. GI (sequence identification number): 2587060, 5′ ccgccATGGCCACCCTGCTC— —ACCAACGCAGAGGACTAGgg 3′ (upper case: coding sequence, lower case: flanking sequence). The scAAV vector construct expressing ribosomal protein L22 tagged with 3xHA (Rpl22-3xHA) driven by the UBC promoter was also made by DNA synthesis of the UBC promoter through Rpl22-3xHA (490 bp) and cloning it into an scAAV backbone plasmid. Similarly, an scAAV-UBC-Null construct that contains no coding sequence was made a control.

The double-floxed inverse open reading frame (DIO) strategy was used to express GAD65 and VGAT driven by the UBC promoter upon Cre-mediated recombination.[45–47] GAD65 and VGAT cDNAs were double floxed at both ends with *loxP* and lox2272, linked inverse orientation with UBC promoter, and the expression cassettes were cloned into a scAAV backbone plasmid, respectively. scAAV9 and scAAV-Anc80 vectors are produced by transient co-transfection of HEK293T cells with three plasmids (each vector construct, pAAV2/Cap9 or pAAV2/CapAnc80, and pAd-helper). Virus titers were measured by quantitative real-time-PCR to determine the genome copy number of the vector preparations as a measure of AAV particles with full genome content (gc/mL).[48,49] The final concentrations of the scAAV9-UBC-GAD65 and scAAV9-UBC-VGAT were 1.1×10^{12} gc/mL and 2.5×10^{12} gc/mL, respectively. scAAV9-UBC-Null was 3.6×10^{12} gc/mL. scAAV9-floxed-GAD65 and scAAV9-floxed-VGAT were 4.0×10^{12} gc/mL and 6.5×10^{12} gc/mL, respectively. scAAV-Anc80-UBC-GAD65 and scAAV-Anc80-UBC-VGAT were 7.5×10^{11} gc/mL and 3.0×10^{12} gc/mL, respectively. scAAV-Anc80-UBC-Null was 5.5×10^{12} gc/mL. scAAV-Anc80- Rpl22-3xHA was 5.5×10^{12} gc/mL. scAAV9-UBC-GFP was 8.0×10^{12} gc/mL. In the mice study, 5% dextran solution was used to dilute the AAV9 or Anc80 vector in a 1:1 ratio, resulting in the final dextran concentration of 2.5%.

Animals

All of the experimental procedures followed the NIH Guidelines or the European Commission Directive (86/609/EEC) and the ethical guidelines of the International Association for the Study of Pain, and were approved by the University of California, San Diego, the local animal ethics committee of the Bogomoletz Institute of Physiology (Kiev, Ukraine), the Institute of Animal Physiology and Genetics, Liběchov, Czech Republic or the local animal ethics committee of the National Primate Research Center of Thailand, Chulalongkorn University (Bangkok, Thailand). B6 (C57BL/6) and FVB (FVB/NJ) mice were purchased from The Jackson Laboratories (Bar Harbor, ME, USA). Vglut2-ires-Cre knockin mice (VGLUT2-Cre) and Vgat-ires-Cre knockin mice (VGAT-Cre) were obtained from S. Paff's laboratory (Salk Institute) and purchased from The Jackson Laboratories. In the pig component of the study, adult Gottingen-Minnesota pigs (25–30 kg; Institute of Animal Physiology and Genetics, Liběchov, Czech Republic) or Yucatan pigs (20–25 kg; UCSD) were used. In the NHP component of the study, adult cynomolgus monkeys (*Macaca fascicularis*) (3–5 kg; the National Primate Research Center of Thailand, Chulalongkorn University, Bangkok, Thailand) were used. Animals had free access to food and drinking water before the experiments. The general health and BW of all of the animals were monitored on a daily basis during the whole experiment.

Induction of neuropathic pain in adult mice

To induce neuropathic pain, a unilateral (right side) sciatic nerve ligation was performed, as previously described.[25] All of the surgical procedures were done under sterile conditions. Briefly, mice were anesthetized with 2%–3% isoflurane, and the surgical area was shaved and cleaned. Under the dissecting microscope, the right sciatic nerve was exposed and half-ligated using 8-0 silk sutures. After sciatic nerve ligation (PNI), muscle and skin incisions were closed using 3.0 Proline. Before recovery from anesthesia, the animals received antibiotics (cefazolin, 10 mg/kg) and the initial dose of pain medication (Buprenex, 0.05 mg/kg).

Experimental design

There were 7 separate components of the study: (1) AAV-vector distribution study in adult B6 mice, (2) anti-nociceptive treatment study in B6 mice, (3) safety profile study in B6 mice, (4) anti-nociceptive treatment study in VGAT-Cre and VGLUT2-Cre mice, (5) *ex vivo* electrophysiology study in FVB mice, (6) AAV-vector distribution and safety study in adult pigs, and (7) NHP.

AAV-vector distribution study in adult B6 mice

Animals (12–20 weeks old; n ≥ 9, male) received unilateral lumbar (L3–L5) subpial injection of progressively increased volume(s) of AAV9-UBC-GFP virus (0.5, 1.0, and 3.0 μL). A separate group of animals (n = 3) received 2 bilateral lumbar subpial injections of AAV9-UBC-GFP virus (3.0 + 3.0 μL). After vector delivery, the animals survived for 2 weeks.

Anti-nociceptive treatment study in B6 mice

Animals (12–13 weeks old; male) were randomly divided into 6 experimental groups: (1) Sham-operated (n = 7), (2) PNI subpially injected

with PBS (0.5 µL, n = 6), (3) PNI subpially injected with AAV-UBC-Null (0.5 µL, n = 7), (4) PNI subpially treated with AAV9-UBC-GAD65 and VGAT (total 0.5 µL, n = 11), (5) PNI subpially treated with AAV9-UBC-GAD65 only (0.5 µL, n = 7), and (6) PNI subpially treated with AAV9-UBC-VGAT only (0.5 µL, n = 7). In a separate experiment, animals (12–13 weeks old; male) were randomly divided into 2 experimental groups: (1) PNI subpially treated with Anc80-UBC-Null (0.5 µL, n = 8) and (2) PNI subpially treated with Anc80-UBC-GAD65 and bupr Anc80-UBC-VGAT (total 0.5 µL, n = 8). This component of the study was designed to study and compare the potency of Anc80 versus AAV9 used as a delivery treatment vector(s). After vector delivery, animals survived between 7 weeks and 13 months. In an additional separate experiment, naive animals (B6 mice) were injected with AAV9-UBC-GAD65 and AAV9-UBC-VGAT (total 1.0 µL) or "null" virus vector (1.0 µL) (n = 4 per group) and survived for 14 days. The ipsilateral dorsal horn tissue was used for WB analysis.

Safety profile study in B6 mice
Animals (12–13 weeks old; male) were randomly divided into 2 experimental groups: (1) WT non-manipulated (n = 8) and (2) WT subpially treated with AAV9-UBC-GAD65 and AAV9-UBC-VGAT (total 0.5 µL, n = 8). This component of the study was designed to examine the safety profile of the injection of AAV9-UBC-GAD65 and AAV9-UBC-VGAT. After vector delivery, the animals survived between 10 weeks and 13 months.

Anti-nociceptive treatment study in VGAT-Cre and VGLUT2-Cre mice
B6 WT mice (n = 7), VGAT-Cre (n = 8), and VGLUT2-Cre (n = 8) mice (12–14 weeks old; male) with PNI were subpially treated with AAV9-UBC-loxed-GAD65 and AAV9-UBC-loxed-VGAT vectors (total 0.5 µL). After vector delivery, the animals survived for 8 weeks.

Ex vivo electrophysiology study in FVB mice
Male FVB mice (12–13 weeks old) were divided into three groups: (1) naive mice (WT) (n = 6), (2) subpially injected with AAV9-UBC-GFP (sham GFP control; 1.6×10^{13} gc/mL; 3.0 µL; n = 6), and (3) subpially injected with AAV9-UBC-GFP, AAV9-UBC-GAD65, and AAV9-UBC-VGAT (GAD65 + VGAT group; 5.3×10^{12} gc/mL, 1.5×10^{12} gc/mL and 3.3×10^{12} gc/mL, respectively; total 3.0 µL; n = 6). Ex vivo slice preparation was performed at 2–5 weeks after subpial injections.

AAV-vector distribution and safety study in adult pigs
Adult pigs (Gottingen-Minnesota, 20–25 kg, or Yucatan, 15–20 kg) were divided into two groups and received lumbar unilateral injections ofl (1) Anc80-Rpl22-3xHA vector (50, 100, or 200 µL; n = 5) or (2) Anc80-UBC-GAD65 and Anc80-UBC-VGAT vector (total 100 µL; n = 3). After vector delivery, the animals survived for 2 days (Anc80-Rpl22-3xHA) or 2 months (Anc80-UBC-GAD65/VGAT).

AAV-vector distribution and safety study in NHP
Adult cynomolgus monkeys (3–5 kg; n = 5: 2 males and 3 females) received lumbar unilateral injections of Anc80-UBC-GAD65 and Anc80-UBC-VGAT vector (total 25–50 µL; n = 5). After vector delivery, the animals survived for 2 months.

Subpial injection procedure
Mice
All of the surgical procedures were done under sterile conditions. A lumbar (L3–L5) subpial vector injection in mice was performed, as previously described.[22] Briefly, mice were anesthetized with 2%–3% isoflurane, the surgical area shaved and cleaned, and skin incision made at the T13–L2 vertebral level. Under the dissecting microscope, a dorsal laminectomy of L1 vertebra was performed and dura overlying the L3–L5 spinal segments were cut open using a 30-G needle. The pia matter was then punctured using a 36-G pia-penetrating needle, followed by the insertion of a blunt 36-G injection needle containing the AAV9 or Anc80 vector into the right dorsal subpial space. Both the pia-penetrating and subpial injection needle are mounted on a fine XYZ manipulator (SMM 100B; Narishige, Tokyo, Japan). The AAV9 or Anc80 vector was then injected into the lumbar subpial space (0.5, 1.0, and 3.0 µL of vector over 60 s) using a 50-µL Hamilton syringe and a digital infusion pump (Microinjector MINJ-PD; Tritech Research, Los Angeles, CA, USA). After vector delivery, the needle was removed and muscle and skin closed using 3.0 Proline. Before recovery from anesthesia, the animals received subcutaneous fluids, antibiotics (cefazolin, 10 mg/kg), and the initial dose of pain medication (Buprenex, 0.05 mg/kg).

Pigs
Adult pigs were premedicated with ketamine (50 mg/kg, intramuscularly [i.m.]) and induced with propofol (0.5 mg/kg/min, intravenously [i.v.]). After endotracheal intubation, anesthesia was maintained with 1.5%–2.5% isoflurane in 50% air/50% oxygen at a constant flow rate of 2 L/min. The dorsal lumbar area was then shaved and cleaned. The skin overlying the L2–L5 vertebrae was cut open. A unilateral laminotomy of L3–L4 vertebrae was then performed using Kerrison laminectomy punches (Figure 6A). The dura mater was then cut open using a scalpel blade, and the dorsal root entry zone of the L4 spinal segment was exposed. Under the dissecting microscope, a bent "pencil-style" needle (27-G, 3 mm length of horizontal subpially placed needle arm) was placed into the subpial space just above the dorsal root entry zone (Figure 6A). The tip of the needle was directed caudally. To place the subpial needle, an XYZ manipulator (Narishige) mounted on a custom-made stainless-steel platform was used. To stabilize the XYZ manipulator-holding platform, the platform was firmly attached to the vertebral column by using titanium spinal clamps (Medtronic, Minneapolis, MN, USA). Anc80-UBC-Rpl22-3xHA or Anc80-UBC-GAD65/VGAT was then infused into the subpial space (amount of vector: 50, 100, or 200 µL, infusion rate: 0.6, 1.5, or 3.0 s/µL; see Figure S9) using a digital microinjector (Tritech Research). After virus delivery, the needle was carefully removed and the dura mater was closed using 6.0 Proline, and muscle and skin were closed using 3.0 Proline. Before recovery from anesthesia, the animals received antibiotics (cefazolin, 500 mg, i.m.) and pain medication (Buprenex, 0.25 mg/kg, i.m.) and were monitored until fully awake. Antibiotic and pain medication treatment continued for 48 h post-surgery.

NHPs

Cynomolgus monkeys (3–5 kg; n = 5: 2 males and 3 females) were premedicated with ketamine (50 mg/kg, i.m.) and induced with propofol (0.5 mg/kg/min, i.v.). After endotracheal intubation, anesthesia was maintained with 1.5%–2.5% isoflurane in 50% air/50% oxygen at a constant flow rate of 2 L/min. The dorsal lumbar area was then shaved and cleaned. The skin overlying the L2–L5 vertebrae was cut open. A unilateral laminotomy of L2–L3 vertebrae was then performed using Kerrison laminectomy punches. The dura mater was then cut open using a scalpel blade, and the dorsal root entry zone of the L4 spinal segment was exposed. Under the dissecting microscope, a bent 30-G pencil-style needle (3 mm length of horizontal subpially placed needle arm) was placed into subpial space just above the dorsal root entry zone. The tip of the needle was directed caudally. To place the subpial needle, an XYZ manipulator (Narishige) mounted on a custom-made external frame was used. The Anc80-UBC-GAD65/VGAT vector was infused into the subpial space (25 or 50 μL, infusion rate: 3.0 s/μL) using a digital microinjector. After virus delivery, the needle was removed and the dura mater was closed using 6.0 Proline; the muscle and skin were closed using 3.0 Proline. Before recovery from anesthesia, the animals received antibiotics (cefazolin, 20 mg/kg, i.v.), pain medication (Buprenex, 0.25 mg/kg, i.m.) and were monitored until fully awake. Antibiotic and pain medication treatment was continued for 48 h post-surgery.

Tactile- and brush-evoked nociceptive response measurement in mice

All of the animals were placed in an elevated chamber with a mesh floor and habituated to the testing circumstance on 3–4 sessions. On each day of the testing, the animals were first habituated to a testing chamber for 1-h before the testing. To measure tactile-evoked nociceptive responses, the center plantar surface of the hind paw was stimulated with calibrated von Frey filaments (0.008–2.0 g). The paw-withdrawal threshold for the tactile-evoked nociceptive response was determined by Dixon's up-down method.[50] To measure brush-evoked nociceptive response, the lateral plantar surface of the hind paw was stimulated by light stroking with a paintbrush (#00, Winsor & Newton, London, UK), in the direction from heel to toe, with a velocity of ∼2 cm/s.[51] The test was repeated 3 times with intervals of 10 s. For each test, no evoked movement was scored as 0, walking away or occasionally brief paw lifting (for 1 s or less) was scored as 1, one strong lateral paw lifting above the level of the body or a startle-like jump was scored as 2, and multiple flinching responses or licking of the stimulated paw was scored as 3. For each animal, the stimulation was repeated 3 times at intervals of at least 3 min, and the average score was calculated. Baseline tactile- and brush-evoked nociceptive responses were assessed before surgery. After the induction, PNI responses were assessed at 2, 5, and 9 days. After subpial vector or PBS injection, both nociceptive tests were performed every week until sacrifice.

Heat-evoked nociceptive response measurement in mice

To measure hind paw withdrawal latencies from a thermal stimulus, a modified Hargreaves-type hot box (Paw Thermal Stimulator System, University of California, San Diego) was used.[52] All of the animals were placed in individual boxes on the hot box glass surface and habituated to the testing circumstance for 3–4 sessions. The glass surface was maintained at 30°C before the measurement. A radiant heat light source was placed under the mouse planter surface, and automatically turned off after 20 s to avoid tissue damage. The animals were then tested three times, and the latencies were recorded automatically. The average latency was calculated and used for subsequent analyses for each animal.

Open field activity test

The open field test was performed to assess the general motor activity (running distance) of animals before and after treatment and to identify a potential treatment-related motor dysfunction. Briefly, an animal was placed in a 34 × 26 × 34-cm plastic box positioned in a dimly lit room with an overhead infrared (IR) video camera connected to personal computer (PC)-based tracking software (EthoVision XT 7.1, Noldus IT, Wageningen, Netherlands). The software monitored the actual animal movement based on a body-centered contrast subtracted from the background. All of the tested animals were released in the center of the plastic box (one animal per box), acclimatized to the room environment for 10 min, and then continuously recorded for a total exploration time of 1 h. A total of six animals were recorded simultaneously during each recording session. The total running distance and anxiety behavior were calculated by using EthoVision XT 7.1 and ArenasTracker software (IEP SAS, Kosice, Slovakia). Anxiety behavior was evaluated as the time spent out of the central area, with dimensions 40% of the total arena's dimensions. The time when the position of the animal (represented by its center of mass) was out of the central zone was registered and presented as a percentage of the total time (10 min in each case).

Rotarod test

To test induced motor activity, the rotarod test was used. The rotarod test was performed on an accelerating rod apparatus (San Diego Instruments, San Diego, CA, USA). For training, the animals were placed on the static rod for 5 min for at least 3 training days. The animals were then tested 2 times on accelerated rod running from 0 to 20 rpm/min, and the latency to animal falling off the rotating rod surface was recorded. The average latency was calculated and used for subsequent analyses for each animal.

CatWalk paw print analysis

Paw placement analysis was performed using the Noldus CatWalk system (Noldus IT). Mice were trained to walk across a clear glass runway without pauses, with walking tracks recorded and analyzed using the EthoVision CatWalk software (Noldus IT). The software setting for detecting the paw signal was determined based on a naive healthy mouse walking pattern. In naive healthy mice, there are typically six paw-glass surface contact points: five finger tips and the center part of the plantar surface of the paw counted as one. The animals were tested three times and the tracks recorded. A pair of hind paw prints, left and right, recorded on the center of the runway was

selected, and hind paw contact points were then counted and used for subsequent analyses for each animal.

Hoffmann reflex and rate-dependent depression recording

Under isoflurane anesthesia, the right hindlimb of an animal was secured, and a pair of stimulating needle electrodes was transcutaneously inserted into the surroundings of the tibial nerve. For recording, a pair of 30-G platinum needle electrodes were inserted into the interosseous muscles between the fourth and the fifth, or the first and the second metatarsal muscles of the right hind paw, and a grounding electrode was placed into the tail. The tibial nerve was stimulated using square pulses with increasing stimulus intensity (0.1–4 mA in 0.2-mA increments, 0.1 Hz, 0.2 ms; DS3 constant current isolated stimulator, Digitimer, Hertfordshire, UK), and responses were recorded with an alternating current (A/C)-coupled differential amplifier (model DP-311, Warner Instruments, Hamden, CT, USA). The amplified signal was acquired by the PowerLab 8/30 data acquisition system (ADInstruments, Colorado Springs, CO, USA) at a sampling frequency of 20 kHz, digitized and stored in a PC for analysis. We used these data to determine the intensity necessary to obtain a maximal M and H response. In the subsequent RDD assay, only the H-max stimulation intensity was used. To measure the RDD of the Hoffmann reflex, trains of 20 pulses delivered at 0.1, 1, and 5 Hz (at H-max stimulation intensity) were used for stimulation, and changes in H-wave amplitude were compared as a percentage difference between stimulation frequencies (percentage change of baseline). The same procedure was performed for the left hindlimb.

Ex vivo spinal cord preparation

FVB mice (10–14 weeks old) were quickly decapitated and the vertebral column cut out and immersed at room temperature into an oxygenated sucrose solution containing (in millimoles) sucrose 200, KCl 2, NaH_2PO_4 1.2, $CaCl_2$ 0.5, $MgCl_2$ 7, $NaHCO_3$ 26, and glucose 11 (pH 7.4 when bubbled with 95% O_2 and 5% CO_2). The spinal cord was gently removed with the attached L5 (occasionally L4 and L5) dorsal root cut close to the corresponding ganglia. The lumbar spinal cord was cleaned from the dura and pia mater, glued with cyanoacrylate adhesive to a metal plate, and then transferred to the recording chamber. Neurons in the region between the dorsolateral funiculus and the dorsal root entry zone[53] were visualized using the oblique IR light-emitting diode (LED) illumination technique.[54,55] The specific equipment used for the implementation of this technique and for the acquisition of fluorescent images was described previously.[56]

Ex vivo electrophysiological recordings

Electrophysiological recordings from Lamina I neurons in the L4–L5 segments of *ex vivo* spinal cord preparation were performed at a room temperature of 20°C–22°C in oxygenated artificial CSF containing (in millimoles) NaCl 125, KCl 2.5, $CaCl_2$ 2, $MgCl_2$ 1, NaH_2PO_4 1.25, $NaHCO_3$ 26, and glucose 10 (pH 7.4, 95% O_2, and 5% CO_2). Patch pipettes were pulled from borosilicate glass using a P-87 horizontal puller (Sutter Instruments, Novato, CA, USA). Pipettes had resistances of 3–5 MΩ when filled with intracellular solution containing

(in millimoles) K-gluconate 145, $MgCl_2$ 2.5, HEPES 10, Na_2-ATP 2, Na-GTP 0.5, and EGTA 0.5 (pH 7.3). Signals were acquired and filtered at 2.6 kHz using the MultiClamp 700B amplifier (Molecular Devices, Sunnyvale, CA, USA) and digitized at 10 kHz with Digidata 1320A under the control of pClamp 9.2 software (Molecular Devices). Offset potentials were compensated for before seal formation. Liquid junction potentials were not compensated for. Recordings were conducted in cell-attached and whole-cell configurations. Cell-attached recordings were performed to assess the genuine (unperturbed) AP firing activity of neurons. Recordings in the voltage clamp mode were carried out at a holding potential of −70 mV to isolate excitatory post-synaptic currents and of −30 mV to acquire both excitatory and inhibitory currents. To assess evoked activity in Lamina I spinal neurons, electrophysiological recordings were coupled with dorsal root stimulations. Spared ipsilateral dorsal roots were stimulated by a suction electrode, with square current pulses produced by a stimulator (ISO-Flex, AMPI, Jerusalem, Israel).[53,56] Supramaximal stimulation (1 ms, 150 μA), activating all of the primary afferents, including nociceptive Aδ and C-fibers, were used in all of the experiments. The isolation of GABAergic currents was performed by blocking glycinergic currents with strychnine (1 μM). Electrophysiological data were analyzed using Clampfit 9.2 software (Molecular Devices). Spontaneous inhibitory post-synaptic currents (sIPSCs) were detected and analyzed using MiniAnalysis software (Synaptosoft, Decatur, GA, USA), as described previously.[57]

Post-mortem tissue collection

Animals were euthanized with pentobarbital (100 mg/kg) and perfused with 20 mL (mice), 3,000 mL (pigs), or 1,000 mL (NHPs) of heparinized saline followed by 20 mL (mice), 3,000 mL (pigs), or 1,000 mL (NHPs) of 4% paraformaldehyde in PBS. The spinal cords, DRGs, and brains were dissected and post-fixed in 4% formaldehyde in PBS overnight at 4°C. Samples for IF staining and mRNA *in situ* hybridization were then cryoprotected for 72 h with 30% sucrose in PBS 1x.

Transparent tissue preparation and 3-dimensional (3D) imaging

The CLARITY method was used for the preparation for transparent spinal cord tissue.[58] Mice were euthanized with pentobarbital (100 mg/kg) and perfused with 20 mL ice-cold PBS 1x followed by 25 mL cold hydrogel solution. The thoracic to lumbar spinal cord was rapidly dissected and kept in a cold hydrogel solution (15 mL) in the dark at 4°C for 24 h. The tissues were then placed in a rotating incubator at 37°C for 3 h. After the polymerization of hydrogel, excess gel on the spinal cords was gently removed, and the tissues were then placed into a clearing solution (50 mL) for 1 to 2 months. The tissues were passively cleared in the clearing solution on a shaker at 37°C. The clearing solution was exchanged every 3 days for up to 1 month. The tissues were then rinsed 3 times in PBS 1x for several days. After the PBS 1x wash, the tissues were transferred into a refractive index matching solution, 88% Histodenz (Sigma-Aldrich, D2158, refractive index 1.46). The tissue was then imaged using a 4× magnification light-sheet fluorescence microscope (Lightsheet Z.1, Carl Zeiss AG, Oberkochen, Germany) to detect GFP+ cells. Acquired images were

processed with Zen Blue 2.3 software (Carl Zeiss AG) and then stitched with TeraStitcher software.[59] The 3D graphics images were assembled using Imaris software (Bitplane AG, Zürich, Switzerland).

IF staining

Cryoprotected spinal cord or brain tissue was embedded in optimal cutting temperature (OCT) matrix compound (Tissue-Tek, Sakura Finetek, Torrance, CA, USA), frozen in dry ice, and mounted in the cryostat. Sections from the spinal cord, DRG, brains, and brainstem were cut at a thickness of 15–30 μm. Free-floating sections were washed 3 times in PBS 1x with 0.3% Triton X-100 (T-X100), followed by a blocking step with 4% serum in PBS 1x with 0.3% T-X100 for 1 h. Sections were then incubated in the primary antibodies (in blocking solution) overnight at 4°C. The following day, the sections were washed 3 times with PBS 1x with 0.3% T-X100 and incubated with a secondary antibody in PBS 1x with 0.3% T-X100 for 1 h at room temperature. Sections were mounted on slides, dried at room temperature, and coverslipped in ProLong Gold antifade mounting media with or without DAPI (Invitrogen, Carlsbad, CA, USA). The following primary antibodies and dilutions were used in mice and pigs: GFP (chicken, Millipore-Sigma, cat. no. ab13970, 1:1,000), GAD65 (mouse, Santa-Cruz, cat. no. sc73650, 1:500), VGAT (rabbit, Synaptic Systems, cat. no. 131002, 1:500), VGLUT2 (guinea pig, Millipore-Sigma, cat. no. AB2251-I, 1:2,000), NeuN (chicken, Millipore-Sigma, cat. no. ABN91, 1:1,000), Iba1 (rabbit, Wako clone NCNP24, cat. no. 019-19741, 1:1,000), NK1R (rabbit, Sigma-Aldrich, cat. no. S8305, dilution 1:5,000), and HA (mouse, Millipore-Sigma, cat. no. H3663, 1:500). The following primary antibodies and dilutions were used in NHPs: GAD65 (guinea pig, Synaptic Systems, cat. no. 198-104, 1:500), VGAT (rabbit, Synaptic Systems, cat. no. 131002, 1:500), VGLUT2 (mouse, Millipore-Sigma, cat. no. MAB5504, 1:500), and HA (rabbit, Cell Signaling Technology, #3724, 1:500). For the detection of primary antibodies, donkey anti-chicken, anti-rabbit, anti-mouse, or anti-guinea pig Cy3, Cy5, Alexa 488, or Alexa 405-conjugated secondary antibodies (Jackson ImmunoResearch, West Grove, PA, USA) diluted 1:1,000 were used.

Tissue preparation for RNA *in situ* hybridization assay

Fixed tissues were embedded in OCT (Tissue-Tek, Sakura Finetek), frozen in dry ice, and mounted in the cryostat. Sections from spinal cord and DRGs were cut at a thickness of 5 μm (BaseScope) or 15 μm (RNAscope) and directly mounted on slides (Superfrost Plus, Thermo Fisher Scientific, Waltham, MA, USA) and left overnight at room temperature to dry.

RNAscope multiplex assay

RNA FISH was performed using the RNAscope Multiplex Fluorescent version 2 (cat. no. 323100, Advanced Cell Diagnostics, Newark, CA, USA) following the fixed frozen tissue protocol according to the manufacturer's instructions. Briefly, the tissues were treated with peroxidase hydrogen blocker before boiling at 98°C–100°C in a pretreatment solution for 10 min. Protease Plus was then applied for 30 min at 40°C. Paired double-Z oligonucleotide probes against target VGAT, GAD65, and VGLUT2 RNA (RNAscope, Mm-Slc32a1: NM_009508.2, 20 pairs, nt 894–2,037; Hs-Slc32a1: NM_080552.2,

20 pairs, nt 553–1 852; Mm-Gad2: NM_008078.2, 20 pairs, nt 552–1,506; Mmu-Gad2: NM_001265854.1, 20 pairs, nt 501–1,628; Mm-Slc17a6: NM_080853.3, 20 pairs, nt 1,986–2,998; Hs-Slc17a6: NM_020346.2, 20 pairs, nt 724–1,689; Advanced Cell Diagnostics) were pre-diluted 1:50 and hybridized for 2 h at 40°C, followed by a series of signal amplification and washing steps. All of the incubation steps at 40°C were performed in the HybEZ Hybridization System. Hybridization signals were detected by a chromogenic reaction using 1:2,000 of Cy5 chromogen for VGAT or GAD65, 1:50 of Cy2 chromogen for GAD65, and 1:2,000 of Cy3 chromogen for VGLUT2 (PerkinElmer TSA Plus Systems, PerkinElmer Life Sciences, Boston, MA, USA). Each sample was quality controlled for RNA integrity with a probe specific to the housekeeping gene cyclophilin B (PPIB), RNA polymerase subunit IIA (PolR2A), and ubiquitin C (UBC) (RNAscope 3-plex Positive Control Probe, cat. no. 320881, Advanced Cell Diagnostics). Negative control background staining was evaluated using a probe specific to the bacterial dapB gene (RNAscope 3-plex negative control probe, cat. no. 320871, Advanced Cell Diagnostics).

BaseScope duplex assay

RNA *in situ* hybridization assays were performed using the Basescope Duplex assay (cat. no. 323810, Advanced Cell Diagnostics) following the manufacturer's protocol. Briefly, the tissues were treated with peroxidase hydrogen blocker before boiling at 98°C–100°C in a pretreatment solution for 10 min. Protease lll was then applied for 30 min at 40°C. Paired double-Z oligonucleotide probes designed to specifically detect AAV-induced VGAT and GAD65 RNA (BaseScope probe; Advanced Cell Diagnostics) were hybridized for 2 h at 40°C, followed by a series of signal amplification and washing steps. All of the incubation steps at 40°C were performed in a HybEZ Hybridization System. Hybridization signals were detected by chromogenic reaction using FAST Red and Green dyes. Slides were counterstained with Gill's hematoxylin and mounted with Vectamount permanent mounting media (cat. no. 321584, Vector Laboratories, Burlingame, CA, USA). Bright-field images were acquired using a microscope (Zeiss AxioImager M2 Microscope, Carl Zeiss) with Stereo investigator software (MBF Bioscience, Williston, VT, USA) using a 20× and 63× objective. Each sample was quality controlled for RNA integrity with a probe specific to the housekeeping gene PPIB and PolR2A (BaseScope Duplex Positive control probe, cat. no. 700121, Advanced Cell Diagnostics). Negative control background staining was evaluated using a probe specific to the bacterial dapB gene (BaseScope negative control probe, cat. no. 701021, Advanced Cell Diagnostics).

Fluorescence microscopy

Fluorescence images were captured using an immunofluorescence microscope (Zeiss AxioImager M2 Microscope, Carl Zeiss) with Stereo investigator software, and confocal images were taken using an Olympus FV1000 microscope (Olympus, Tokyo, Japan). Confocal images were then processed with Olympus FV10-ASW Viewer software where Z-projections from 10–30 optical sections with 0.3- to 0.5-μm steps were compiled. Identical settings were kept across all of the sections and microscopy sessions. Mosaic images were captured

from complete brain and spinal cord sections at the desired wavelength or spectrum of light from each independent channel to obtain the best focal plane.

Quantitative densitometry in IF-stained sections

Spinal cord sections (30 μm transverse, free-floating) from thoracic (T13 segment) and lumbar (L1–L5 segments) were stained side by side with the GAD65, VGAT, and VGLUT2 antibodies, respectively. Three sections per segment were selected, with at least 210-μm spacing. DRG sections (15 μm transverse, on-slide) from lumbar (L4, L5 segments) were stained side by side with the Iba1 antibody. Dorsal horn and DRG images of whole transverse sections were acquired at 10× or 20× using a Zeiss Imager M2 microscope (Carl Zeiss) and Stereo Investigator software (MBF Biosciences). Identical camera and fluorescent light source settings were used across all of the sections and microscopy sessions. The images were converted to grayscale, and the border of the dorsal horn was outlined. White binary and the mean gray value of GAD65, VGAT, VGLUT2, and Iba1 antibodies signals were then measured using ImageJ software.

EM

Fixed tissues with 4% paraformaldehyde in PBS 1x were washed with 0.15 M glycine/phosphate buffer, embedded in 10% gelatin/phosphate buffer, and infused with 2.3 M sucrose/phosphate buffer overnight at 4°C. The 1-mm^3 tissue blocks were mounted onto specimen holders and snap frozen in liquid nitrogen. Ultracryomicrotomy was carried out at −100°C on a Leica Ultracut UCT with EM FC7 cryo attachment (Leica, Bannockburn, IL, USA) using a Diatome diamond knife (Diatome US, Hatfield, PA, USA). We picked up 80- to 90-nm frozen sections with a 1:1 mixture of 2.3 M sucrose and 2% methyl-cellulose (15 cp)[60] and transferred onto Formvar and carbon-coated copper grids. Immunolabeling was performed by a slight modification of the Tokuyasu technique.[61] Briefly, grids were placed on 2% gelatin at 37°C for 20 min, rinsed with 0.15 M glycine/PBS, and the sections were blocked using 1% cold water fish skin gelatin. Previously titrated primary antibodies were diluted in 1% BSA/PBS. Incubation with primary antibodies, GAD65 (mouse, Santa Cruz, cat. no. sc73650, 1:2,000), VGAT (rabbit, Synaptic Systems, cat. no. 131002, 1:2,000), VGLUT2 (guinea pig, Millipore-Sigma, cat. no. AB2251-I, 1:3,000), for 1 h at room temperature was followed by gold conjugated goat anti-mouse immunoglobulin G (IgG) and IgM (Jackson ImmunoResearch), gold conjugated goat anti-rabbit IgG, or gold conjugated goat anti-guinea pig IgG, all diluted 1/25 in 1% BSA/PBS at room temperature for 30 min. Grids were viewed using a JEOL JEM-1400Plus (JEOL, Peabody, MA, USA) transmission electron microscope and photographed using a Gatan OneView digital camera (Gatan, Pleasanton, CA, USA).

Quantitative analysis for immune-EM images

In double-label immuno-EM for VGLUT2 and GAD65 or VGAT, we analyzed synaptic terminals at a magnification of 3,000–6,000×. The images of excitatory and inhibitory terminals were then taken at a magnification of 10,000–20,000×. Ten images from excitatory and inhibitory terminals were taken from two experimental groups: PNI

treated with PBS and PNI treated with AAV9-UBC-GAD65 and AAV9-UBC-VGAT. The number of immune-gold particles positive for VGLUT2, GAD65, and VGAT in the terminals was counted manually and expressed as an average of counted terminals per 0.25 μm^2. ImageJ software was used for the area calculation.

DRG semithin section preparation and staining

Each DRG was postfixed in 1% osmium tetroxide and embedded into Durcupan according to the standard protocol. The orientation of the ganglion was random. Serial sections (1 μm thick) were cut with a sliding microtome (Leica SM2010R) using a special blade for hard materials (Feather N35HR), (CellPath, 80 Mochdre Enterprise Park Newtown, Powys, SY16 4LE UK). Every 20th section was pulled onto gelatin-coated slides from 90% ethanol and dried at 60°C, so that from each ganglion a series of sections at 20 μm distances was collected (17–32 sections) for further analysis. The sections were stained according to Richardson's staining protocol[62] and coverslipped with Poly-Mount (Polysciences, Inc, Warrington, PA, USA).

DRG volumetric analysis

Stained sections taken from the DRGs were scanned using a digital pathology slide scanner Aperio AT2 (Leica) at maximal resolution (40×). On the digitalized image from each section, the cellular portion of the ganglion was outlined and the area measured with the aid of ImageJ software. The volume of the ganglion was then estimated using the Cavalieri principle; the fibrous portion of the hilum was not included.

mRNA sequencing

Total RNA was isolated from flash-frozen ipsilateral and contralateral dorsal spinal cord samples using the Qiagen RNeasy Plus Mini Kit. A total of 1–2 μg RNA was isolated from each sample, with RNA integrity number (RIN) scores over 8 for all of the samples (most samples had RIN scores over 9), as determined by TapeStation analysis (Agilent Technologies, Santa Clara, CA, USA). SR75 mRNA sequencing libraries were prepared using the Illumina Stranded mRNA Library kit and sequenced on the Illumina HiSeq4000 platform at the sequencing core at the UCSD IGM Genomics Center. Single-end 75-bp reads (average 20 million reads per sample) were received in FASTQ format and were prepared for downstream analysis by trimming known barcodes and then selecting post-trimmed reads for those with an average base quality >15. Reads were aligned to the mouse genome (mm10) using STAR. Successfully aligned reads were then quantified using Kallisto against the Gencode (M17) transcript database. Heatmaps were generated in R with the 'pheatmap' package.

WB analysis

Lumbar spinal segment of 4 animals per group (AAV9-UBI-GAD65 + VGAT-injected, null virus injected and naive control) were homogenized in ice-cold lysis buffer (NP-40 0.2%, Mini cOmplete EDTA-free 1.5×, β-mercaptoethanol 0.02 M, and PMSF 10 mM), and centrifuged at 14,000 rpm for 15 min at 4°C. The supernatant fraction was transferred to a clean tube. The protein concentration was measured using the BCA assay (Pierce BCA protein assay

kit, cat. no. 23225, Thermo Fisher Scientific). Fifteen micrograms of protein were prepared and resolved in a 4%–12% Bis-Tris Plus Gel (Invitrogen Bolt) and transferred to polyvinylidene difluoride (PVDF) membranes. The membranes were blocked with 5% non-fat milk in Tris-buffered saline at pH 7.4 (20 mM Tris, 150 mM NaCl, and dH$_2$O) with Tween 1%, and they were incubated with VGAT antibody cytoplasmic domain (rabbit, SYSY cat. no. 131 003, 1:500) or anti-GAD-65 antibody (A3) (mouse, Santa Cruz cat. no. sc-377145, 1:100). For detecting primary antibody an anti-rabbit IgG (Cell signaling # 7074S, 1:10,000) or an anti-mouse (Cell Signaling Technologies cat. no. 7076S, 1:10,000) horseradish peroxidase-linked antibodies were used. The signal of the VGAT and GAD65 were detected using an enhanced chemiluminescence detection system according to the manufacturer's instructions (Millipore, Billerica, MA, USA). Blots were stripped and incubated with a monoclonal antibody directed against HSP90 (C45G5) mAb (rabbit, Cell Signaling Technologies cat. no. 4877 1:1,000), which was used as an internal control to normalize VGAT and GAD65 protein expression levels.

Statistical analysis

Data were analyzed using the EZR software package (Saitama MedicalCenter/Jichi Medical University, Saitama, Japan), R software (R Foundation for Statistical Computing, Vienna, Austria), and Prism 7 software (GraphPad Software, San Diego, CA, USA). As noted in the figure legends, normally (parametric) distributed data were analyzed using the Student's t test for the paired data, or one-way ANOVA or two-way repeated ANOVA followed by Bonferroni's or Tukey's post hoc tests. Non-normally (nonparametric) distributed data were analyzed using the Mann-Whitney U test or the Kolmogorov-Smirnov test for the paired data, or the Kruskal-Wallis test followed by the Mann-Whitney U test with Bonferroni adjustment for multiple comparisons. All of the significance tests were two sided. The number of experiments (n) and significance are reported in the figure legends. The statistical significance of the categorical data was assessed with Fisher's exact test. The datasets were probed for normality using the Shapiro-Wilk test or assumed equal variance and normally distributed data within experimental paradigms where comparisons are made. The data were presented as means ± SEMs, as noted in the figure legends. No statistical methods were used to predetermine the sample size. The sample sizes for the animal behavioral tests were determined based on previous experience with these assays as the minimum number of independent observations required for statistically significant results. For behavioral experiments, animals were randomly chosen for different experimental cohorts by a blinded investigator. The tactile-evoked nociceptive response in AAV9-vector-injected animals (Figure 1C) was evaluated by two independent investigators in a blinded fashion. A p value of less than 0.05 was considered significant for either test.

SUPPLEMENTAL INFORMATION

Supplemental information can be found online at https://doi.org/10.1016/j.ymthe.2022.04.023.

AUTHOR CONTRIBUTIONS

T.T. and M.B.-H. performed the *in vivo* part of the study. T.T., M.B.-H., M.N., and M.S. performed the IF staining and the quantitative and qualitative IF image analysis and FISH assay. K.A., O.P., and V.K. performed the *in vitro* and *in vivo* electrophysiological recordings. Y.K., T.Y., S.J., J.J., H.S., V.P., T.K., D.N., and S.M. performed or assisted in the large-animal surgeries. A.M. produced and validated the AAV9 and Anc80 vectors. S.P.D., T.D.G., and S.L.P. conducted the mRNA sequencing analysis. M.M. designed the study and prepared the manuscript. P.B., J.C., S.L.P., R.R., Z.T., I.V., S.M., J.M., H.K.S., and M.K. contributed to the manuscript preparation. S.M. conducted the project management. All of the authors contributed to the final editing and approval of the manuscript.

DECLARATION OF INTERESTS

M.M. is a co-founder of Neurgain Technologies.

REFERENCES

1. Widerstrom-Noga, E. (2017). Neuropathic pain and spinal cord injury: phenotypes and pharmacological management. Drugs *77*, 967–984. https://doi.org/10.1007/s40265-017-0747-8.

2. Warner, F., Cragg, J.J., Jutzeler, C., Finnerup, N., Werhagen, L., Weidner, N., Maier, D., Kalke, Y.B., Curt, A., and Kramer, J. (2018). The progression of neuropathic pain after acute spinal cord injury: a meta-analysis and framework for clinical trials. J Neurotrauma *36*, 1461–1468. https://doi.org/10.1089/neu.2018.5960.

3. Alles, S.R.A., and Smith, P.A. (2018). Etiology and pharmacology of neuropathic pain. Pharmacol. Rev. *70*, 315–347. https://doi.org/10.1124/pr.117.014399.

4. Felix, E.R. (2014). Chronic neuropathic pain in SCI. Phys. Med. Rehabil. Clin. N. Am. *25*, 545–571. viii. https://doi.org/10.1016/j.pmr.2014.04.007.

5. Jensen, T.S., Madsen, C.S., and Finnerup, N.B. (2009). Pharmacology and treatment of neuropathic pains. Curr. Opin. Neurol. *22*, 467–474. https://doi.org/10.1097/WCO.0b013e3283311e13.

6. DeFrates, S., and Cook, A.M. (2011). Pharmacologic treatment of neuropathic pain following spinal cord injury. Orthopedics *34*, 203–207. https://doi.org/10.3928/01477447-20110124-19.

7. Koulousakis, A., Kuchta, J., Bayarassou, A., and Sturm, V. (2007). Intrathecal opioids for intractable pain syndromes. Acta Neurochir Suppl. *97*, 43–48. https://doi.org/10.1007/978-3-211-33079-1_5.

8. Siniscalco, D., de Novellis, V., Rossi, F., and Maione, S. (2005). Neuropathic pain: is the end of suffering starting in the gene therapy? Curr. Drug Targets *6*, 75–80. https://doi.org/10.2174/1389450053344966.

9. Lee, B., Kim, J., Kim, S.J., Lee, H., and Chang, J.W. (2007). Constitutive GABA expression via a recombinant adeno-associated virus consistently attenuates neuropathic pain. Biochem. Biophys. Res. Commun. *357*, 971–976. https://doi.org/10.1016/j.bbrc.2007.04.061.

10. Yang, F.R., Chen, J., Yi, H., Peng, L.Y., Hu, X.L., and Guo, Q.L. (2019). MicroRNA-7a ameliorates neuropathic pain in a rat model of spinal nerve ligation *via* the neurofilament light polypeptide-dependent signal transducer and activator of transcription

signaling pathway. Mol. Pain *15*. 174480691984246. https://doi.org/10.1177/1744806919842464.

11. Samad, O.A., Tan, A.M., Cheng, X., Foster, E., Dib-Hajj, S.D., and Waxman, S.G. (2013). Virus-mediated shRNA knockdown of Na(v)1.3 in rat dorsal root ganglion attenuates nerve injury-induced neuropathic pain. Mol. Ther. *21*, 49–56. https://doi.org/10.1038/mt.2012.169.

12. Chen, L., Huang, J., Zhao, P., Persson, A.K., Dib-Hajj, F.B., Cheng, X., Tan, A., Waxman, S.G., and Dib-Hajj, S.D. (2018). Conditional knockout of NaV1.6 in adult mice ameliorates neuropathic pain. Sci. Rep. *8*, 3845. https://doi.org/10.1038/s41598-018-22216-w.

13. Hirai, T., Enomoto, M., Kaburagi, H., Sotome, S., Yoshida-Tanaka, K., Ukegawa, M., Kuwahara, H., Yamamoto, M., Tajiri, M., Miyata, H., et al. (2014). Intrathecal AAV serotype 9-mediated delivery of shRNA against TRPV1 attenuates thermal hyperalgesia in a mouse model of peripheral nerve injury. Mol. Ther. *22*, 409–419. https://doi.org/10.1038/mt.2013.247.

14. Fischer, G., Pan, B., Vilceanu, D., Hogan, Q.H., and Yu, H. (2014). Sustained relief of neuropathic pain by AAV-targeted expression of CBD3 peptide in rat dorsal root ganglion. Gene Ther. *21*, 44–51. https://doi.org/10.1038/gt.2013.56.

15. Towne, C., Pertin, M., Beggah, A.T., Aebischer, P., and Decosterd, I. (2009). Recombinant adeno-associated virus serotype 6 (rAAV2/6)-mediated gene transfer to nociceptive neurons through different routes of delivery. Mol. Pain *5*, 52. https://doi.org/10.1186/1744-8069-5-52.

16. Miyanohara, A., Kamizato, K., Juhas, S., Juhasova, J., Navarro, M., Marsala, S., Lukacova, N., Hruska-Plochan, M., Curtis, E., Gabel, B., et al. (2016). Potent spinal parenchymal AAV9-mediated gene delivery by subpial injection in adult rats and pigs. Mol. Ther. Methods Clin. Dev. *3*, 16046. https://doi.org/10.1038/mtm.2016.46.

17. Vulchanova, L., Schuster, D.J., Belur, L.R., Riedl, M.S., Podetz-Pedersen, K.M., Kitto, K.F., Wilcox, G.L., McIvor, R.S., and Fairbanks, C.A. (2010). Differential adeno-associated virus mediated gene transfer to sensory neurons following intrathecal delivery by direct lumbar puncture. Mol. Pain *6*, 31. https://doi.org/10.1186/1744-8069-6-31.

18. Yu, H., Fischer, G., and Hogan, Q.H. (2016). AAV-mediated gene transfer to dorsal root ganglion. Methods Mol. Biol. *1382*, 251–261. https://doi.org/10.1007/978-1-4939-3271-9_18.

19. Wu, H., Jin, Y., Buddhala, C., Osterhaus, G., Cohen, E., Jin, H., Wei, J., Davis, K., Obata, K., and Wu, J.Y. (2007). Role of glutamate decarboxylase (GAD) isoform, GAD65, in GABA synthesis and transport into synaptic vesicles-Evidence from GAD65-knockout mice studies. Brain Res. *1154*, 80–83. https://doi.org/10.1016/j.brainres.2007.04.008.

20. Saito, K., Kakizaki, T., Hayashi, R., Nishimaru, H., Furukawa, T., Nakazato, Y., Takamori, S., Ebihara, S., Uematsu, M., Mishina, M., et al. (2010). The physiological roles of vesicular GABA transporter during embryonic development: a study using knockout mice. Mol. Brain *3*, 40. https://doi.org/10.1186/1756-6606-3-40.

21. Wojcik, S.M., Katsurabayashi, S., Guillemin, I., Friauf, E., Rosenmund, C., Brose, N., and Rhee, J.S. (2006). A shared vesicular carrier allows synaptic corelease of GABA and glycine. Neuron *50*, 575–587. https://doi.org/10.1016/j.neuron.2006.04.016.

22. Tadokoro, T., Miyanohara, A., Navarro, M., Kamizato, K., Juhas, S., Juhasova, J., Marsala, S., Platoshyn, O., Curtis, E., Gabel, B., et al. (2017). Subpial adeno-associated virus 9 (AAV9) vector delivery in adult mice. J. Vis. Exp. *125*, 55770. https://doi.org/10.3791/55770.

23. Bravo-Hernandez, M., Tadokoro, T., Navarro, M.R., Platoshyn, O., Kobayashi, Y., Marsala, S., Miyanohara, A., Juhas, S., Juhasova, J., Skalnikova, H., et al. (2020). Spinal subpial delivery of AAV9 enables widespread gene silencing and blocks motoneuron degeneration in ALS. Nat. Med. *26*, 118–130. https://doi.org/10.1038/s41591-019-0674-1.

24. Bravo-Hernandez, M., Tadokoro, T., and Marsala, M. (2019). Subpial AAV delivery for spinal parenchymal gene regulation in adult mammals. Methods Mol. Biol. *1950*, 209–233. https://doi.org/10.1007/978-1-4939-9139-6_12.

25. Seltzer, Z., Dubner, R., and Shir, Y. (1990). A novel behavioral model of neuropathic pain disorders produced in rats by partial sciatic nerve injury. Pain *43*, 205–218. https://doi.org/10.1016/0304-3959(90)91074-s.

26. Kakinohana, O., Hefferan, M.P., Nakamura, S., Kakinohana, M., Galik, J., Tomori, Z., Marsala, J., Yaksh, T.L., and Marsala, M. (2006). Development of GABA-sensitive spasticity and rigidity in rats after transient spinal cord ischemia: a qualitative and quantitative electrophysiological and histopathological study. Neuroscience *141*, 1569–1583. https://doi.org/10.1016/j.neuroscience.2006.04.083.

27. Luz, L.L., Szucs, P., and Safronov, B.V. (2014). Peripherally driven low-threshold inhibitory inputs to lamina I local-circuit and projection neurones: a new circuit for gating pain responses. J. Physiol. *592*, 1519–1534. https://doi.org/10.1113/jphysiol.2013.269472.

28. Todd, A.J. (2010). Neuronal circuitry for pain processing in the dorsal horn. Nat. Rev. Neurosci. *11*, 823–836. https://doi.org/10.1038/nrn2947.

29. Todd, A.J., Puskar, Z., Spike, R.C., Hughes, C., Watt, C., and Forrest, L. (2002). Projection neurons in lamina I of rat spinal cord with the neurokinin 1 receptor are selectively innervated by substance p-containing afferents and respond to noxious stimulation. J. Neurosci. *22*, 4103–4113. https://doi.org/10.1523/jneurosci.22-10-04103.2002.

30. Marshall, G.E., Shehab, S.A., Spike, R.C., and Todd, A.J. (1996). Neurokinin-1 receptors on lumbar spinothalamic neurons in the rat. Neuroscience *72*, 255–263. https://doi.org/10.1016/0306-4522(95)00558-7.

31. Hains, B.C., and Waxman, S.G. (2006). Activated microglia contribute to the maintenance of chronic pain after spinal cord injury. J. Neurosci. *26*, 4308–4317. https://doi.org/10.1523/JNEUROSCI.0003-06.2006.

32. Shibata, K., Sugawara, T., Fujishita, K., Shinozaki, Y., Matsukawa, T., Suzuki, T., and Koizumi, S. (2011). The astrocyte-targeted therapy by Bushi for the neuropathic pain in mice. PLoS One *6*, e23510. https://doi.org/10.1371/journal.pone.0023510.

33. Stuesse, S.L., Cruce, W.L., Lovell, J.A., McBurney, D.L., and Crisp, T. (2000). Microglial proliferation in the spinal cord of aged rats with a sciatic nerve injury. Neurosci. Lett. *287*, 121–124. https://doi.org/10.1016/s0304-3940(00)01142-3.

34. Calvo, M., Zhu, N., Grist, J., Ma, Z., Loeb, J.A., and Bennett, D.L.H. (2011). Following nerve injury neuregulin-1 drives microglial proliferation and neuropathic pain via the MEK/ERK pathway. Glia *59*, 554–568. https://doi.org/10.1002/glia.21124.

35. Root, D.H., Zhang, S., Barker, D.J., Miranda-Barrientos, J., Liu, B., Wang, H.L., and Morales, M. (2018). Selective brain distribution and distinctive synaptic architecture of dual glutamatergic-GABAergic neurons. Cell Rep. *23*, 3465–3479. https://doi.org/10.1016/j.celrep.2018.05.063.

36. Tritsch, N.X., Granger, A.J., and Sabatini, B.L. (2016). Mechanisms and functions of GABA co-release. Nat. Rev. Neurosci. *17*, 139–145. https://doi.org/10.1038/nrn.2015.21.

37. Zhang, J.M., and An, J. (2007). Cytokines, inflammation, and pain. Int. Anesthesiol. Clin. *45*, 27–37. https://doi.org/10.1097/AIA.0b013e318034194e.

38. Peng, J., Gu, N., Zhou, L., B Eyo, U., Murugan, M., Gan, W.B., and Wu, L.J. (2016). Microglia and monocytes synergistically promote the transition from acute to chronic pain after nerve injury. Nat. Commun. *7*, 12029. https://doi.org/10.1038/ncomms12029.

39. Liu, T., Gao, Y.J., and Ji, R.R. (2012). Emerging role of Toll-like receptors in the control of pain and itch. Neurosci. Bull *28*, 131–144. https://doi.org/10.1007/s12264-012-1219-5.

40. Stokes, J.A., Corr, M., and Yaksh, T.L. (2013). Spinal Toll-like receptor signaling and nociceptive processing: regulatory balance between TIRAP and TRIF cascades mediated by TNF and IFNβ. Pain *154*, 733–742. https://doi.org/10.1016/j.pain.2013.01.012.

41. Svensson, C.I., Marsala, M., Westerlund, A., Calcutt, N.A., Campana, W.M., Freshwater, J.D., Catalano, R., Feng, Y., Protter, A.A., Scott, B., and Yaksh, T.L. (2003). Activation of p38 mitogen-activated protein kinase in spinal microglia is a critical link in inflammation-induced spinal pain processing. J. Neurochem. *86*, 1534–1544. https://doi.org/10.1046/j.1471-4159.2003.01969.x.

42. Yang, L.C., Marsala, M., and Yaksh, T.L. (1996). Characterization of time course of spinal amino acids, citrulline and PGE2 release after carrageenan/kaolin-induced knee joint inflammation: a chronic microdialysis study. Pain *67*, 345–354. https://doi.org/10.1016/0304-3959(96)03106-5.

43. Schafers, M., Marziniak, M., Sorkin, L.S., Yaksh, T.L., and Sommer, C. (2004). Cyclooxygenase inhibition in nerve-injury- and TNF-induced hyperalgesia in the rat. Exp. Neurol. *185*, 160–168. https://doi.org/10.1016/j.expneurol.2003.09.015.

44. Saito, O., Svensson, C.I., Buczynski, M.W., Wegner, K., Hua, X.Y., Codeluppi, S., Schaloske, R.H., Deems, R.A., Dennis, E.A., and Yaksh, T.L. (2010). Spinal glial TLR4-mediated nociception and production of prostaglandin E(2) and TNF. Br. J. Pharmacol. *160*, 1754–1764. https://doi.org/10.1111/j.1476-5381.2010.00811.x.

45. Schnutgen, F., Doerflinger, N., Calleja, C., Wendling, O., Chambon, P., and Ghyselinck, N.B. (2003). A directional strategy for monitoring Cre-mediated recombination at the cellular level in the mouse. Nat. Biotechnol. 21, 562–565. https://doi.org/10.1038/nbt811.

46. Saunders, A., and Sabatini, B.L. (2015). Cre activated and inactivated recombinant adeno-associated viral vectors for neuronal anatomical tracing or activity manipulation. Curr. Protoc. Neurosci. 72, 24.1–1.24.15. https://doi.org/10.1002/0471142301.ns0124s72.

47. Lee, G., and Saito, I. (1998). Role of nucleotide sequences of loxP spacer region in Cre-mediated recombination. Gene 216, 55–65. https://doi.org/10.1016/s0378-1119(98)00325-4.

48. Fang, H., Lai, N.C., Gao, M.H., Miyanohara, A., Roth, D.M., Tang, T., and Hammond, H.K. (2012). Comparison of adeno-associated virus serotypes and delivery methods for cardiac gene transfer. Hum. Gene Ther. Methods 23, 234–241. https://doi.org/10.1089/hgtb.2012.105.

49. Xu, Q., Chou, B., Fitzsimmons, B., Miyanohara, A., Shubayev, V., Santucci, C., Hefferan, M., Marsala, M., and Hua, X.Y. (2012). In vivo gene knockdown in rat dorsal root ganglia mediated by self-complementary adeno-associated virus serotype 5 following intrathecal delivery. PLoS One 7, e32581. https://doi.org/10.1371/journal.pone.0032581.

50. Chaplan, S.R., Bach, F.W., Pogrel, J.W., Chung, J.M., and Yaksh, T.L. (1994). Quantitative assessment of tactile allodynia in the rat paw. J. Neurosci. Methods 53, 55–63. https://doi.org/10.1016/0165-0270(94)90144-9.

51. Cheng, L., Duan, B., Huang, T., Zhang, Y., Chen, Y., Britz, O., Garcia-Campmany, L., Ren, X., Vong, L., Lowell, B.B., et al. (2017). Identification of spinal circuits involved in touch-evoked dynamic mechanical pain. Nat. Neurosci. 20, 804–814. https://doi.org/10.1038/nn.4549.

52. Hargreaves, K., Dubner, R., Brown, F., Flores, C., and Joris, J. (1988). A new and sensitive method for measuring thermal nociception in cutaneous hyperalgesia. Pain 32, 77–88. https://doi.org/10.1016/0304-3959(88)90026-7.

53. Pinto, V., Szucs, P., Lima, D., and Safronov, B.V. (2010). Multisegmental A - and C-fiber input to neurons in lamina I and the lateral spinal nucleus. J. Neurosci. 30, 2384–2395. https://doi.org/10.1523/JNEUROSCI.3445-09.2010.

54. Safronov, B.V., Pinto, V., and Derkach, V.A. (2007). High-resolution single-cell imaging for functional studies in the whole brain and spinal cord and thick tissue blocks using light-emitting diode illumination. J. Neurosci. Methods 164, 292–298. https://doi.org/10.1016/j.jneumeth.2007.05.010.

55. Szucs, P., Pinto, V., and Safronov, B.V. (2009). Advanced technique of infrared LED imaging of unstained cells and intracellular structures in isolated spinal cord, brainstem, ganglia and cerebellum. J. Neurosci. Methods 177, 369–380. https://doi.org/10.1016/j.jneumeth.2008.10.024.

56. Krotov, V., Tokhtamysh, A., Kopach, O., Dromaretsky, A., Sheremet, Y., Belan, P., and Voitenko, N. (2017). Functional characterization of lamina X neurons in ex-vivo spinal cord preparation. Front. Cell Neurosci. 11, 342. https://doi.org/10.3389/fncel.2017.00342.

57. Kopach, O., Krotov, V., Belan, P., and Voitenko, N. (2015). Inflammatory-induced changes in synaptic drive and postsynaptic AMPARs in lamina II dorsal horn neurons are cell-type specific. Pain 156, 428–438. https://doi.org/10.1097/01.j.pain.0000460318.65734.00.

58. Epp, J.R., Niibori, Y., Liz Hsiang, H.L., Mercaldo, V., Deisseroth, K., Josselyn, S.A., and Frankland, P.W. (2015). Optimization of CLARITY for clearing whole-brain and other intact organs. eNeuro. 2. https://doi.org/10.1523/ENEURO.0022-15.2015.

59. Bria, A., and Iannello, G. (2012). TeraStitcher - a tool for fast automatic 3D-stitching of teravoxel-sized microscopy images. BMC Bioinformatics 13, 316. https://doi.org/10.1186/1471-2105-13-316.

60. Liou, W., Geuze, H.J., and Slot, J.W. (1996). Improving structural integrity of cryosections for immunogold labeling. Histochem. Cell Biol. 106, 41–58. https://doi.org/10.1007/bf02473201.

61. Tokuyasu, K.T. (1980). Immunochemistry on ultrathin frozen sections. Histochem. J. 12, 381–403. https://doi.org/10.1007/bf01011956.

62. Richardson, K.C., Jarett, L., and Finke, E.H. (1960). Embedding in epoxy resins for ultrathin sectioning in electron microscopy. Stain Technol. 35, 313–323. https://doi.org/10.3109/10520296009114754.